JOURNAL OF GEOPHYSICAL RESEARCH, VOL. 102, NO. B5, PAGES 10,013-10,037, MAY 10, 1997

Tertiary diachronic extrusion and deformation of western Indochina: Structural and $^{40}Ar/^{39}Ar$ evidence from NW Thailand

Robin Lacassin,[1] Henri Maluski,[2] P. Hervé Leloup,[1] Paul Tapponnier,[1] Chaiyan Hinthong,[3] Kanchit Siribhakdi,[3] Saengathit Chuaviroj,[3] and Adul Charoenravat[3]

Abstract. The Wang Chao and Three Pagodas fault zones cut the western part of the Indochina block and run parallel to the Red River Fault. Evidence of intense ductile left-lateral shear is found in the Lansang gneisses, which form a 5 km wide elongated core along the Wang Chao fault zone. Dating by $^{40}Ar/^{39}Ar$ shows that such deformation probably terminated around 30.5 Ma. The Wang Chao and Three Pagodas faults offset the north striking lower Mesozoic metamorphic and magmatic belt of northern Thailand. $^{40}Ar/^{39}Ar$ results suggest that this belt suffered rapid cooling in the Tertiary, probably around 23 Ma. These results imply that the extrusion of the southwestern part of Indochina occurred in the upper Eocene–lower Oligocene. It probably induced rifting in some basins of the Gulf of Thailand and in the Malay and Mekong basins. In the Oligo–Miocene, the continuing penetration of India into Asia culminated with the extrusion of all of Indochina along the Ailao Shan – Red River fault. This occurred concurrently with the onset of E–W extension more to the south. Plotting in a geographical reference frame the diachronic time spans of movement on left-lateral faults east and southeast of Tibet implies that the northward movement of the Indian indenter successively initiated new strike–slip faults located farther and farther north along its path.

Introduction

The indentation of India into Asia has induced large strain in Tibet and adjacent regions. In regions directly facing the Indian indenter, geophysical and geological evidence bring forth the importance of N–S crustal shortening. India's penetration has also produced a large amount of deformation on the sides of the collision zone. In particular, a part of the convergence has been taken up by the eastward expulsion of continent-size blocks away from the path of India [*Tapponnier et al.*, 1982, 1986; *Peltzer and Tapponnier*, 1988; *Armijo et al.*, 1989]. By successively pushing Indochina and Tibet/South China toward the ESE along great sinistral strike–slip faults, India removed a significant volume of Asian lithosphere from the frontal collision zone. This allowed transfer of part of the convergence–induced shortening toward the East. By the way of strike–slip motion, such shortening was transformed into crustal extension, seafloor spreading, and ultimately subduction near the eastern tips of the strike–slip faults [*Tapponnier et al.*, 1986; *Peltzer and Tapponnier*, 1988; *Briais et al.*, 1993]. One crucial tenet of this model, the Tertiary extrusion of Indochina and the concurrent opening of the South China Sea, is now corroborated by field and laboratory evidence on rocks of the Ailao Shan–Red River shear zone along the northern boundary of Indochina. Along this 1000 km long zone, 700 ±200 km of sinistral motion occurred between ≈35 Ma and 17 Ma [*Schärer et al.*, 1990; *Harrison et al.*, 1992; *Schärer et al.*, 1994] by ductile shear within a 10 to 20 km wide zone [*Tapponnier et al.*, 1990a; *Leloup et al.*, 1995]. In Yunnan, this Cenozoic left–lateral shear, and the coeval ≈E–W shortening are the clearest Phanerozoic tectonic events. More to the South, within Indochina, the major deformation phases are reported to be of Paleozoic or lower Mesozoic age [*Bunopas*, 1981; *Sengör and Hsü*, 1984; *Hahn et al.*, 1986; *Hutchinson*, 1989; *Ahrendt et al.*, 1993; *Maluski et al.*, 1995a], but the importance of the Tertiary imprint remains to be assessed. The ages of the strike–slip faults and shear zones that affect the Indochina block (Figure 1) are poorly constrained. Were such faults initiated by the India–Asia collision, as postulated by *Tapponnier et al.* [1986] ? Was there north–south diachronism, from Thailand to eastern Tibet, in the onset of left–lateral strike–slip faulting? Finally, was the opening of the Cenozoic basins of the Gulf of Thailand and of northern Thailand coeval with such strike–slip movements? As a step to answer those questions, and to better understand the timing of extrusion on the east side of India, we present here a structural analysis of the Wang Chao and Three Pagodas fault zones of NW Thailand, combined with $^{40}Ar/^{39}Ar$ dating in these zones and adjacent to them.

[1] Laboratoire de Tectonique, Mécanique de la Lithosphère; URA 1093, Centre National de la Recherche Scientifique, Institut de Physique du Globe de Paris.

[2] Laboratoire de Géochronologie Géochimie et Pétrologie, URA 5563, Centre National de la Recherche Scientifique, Université Montpellier.

[3] Geological Survey Division, Department of Mineral Resources, Bangkok, Thailand.

Paper number 96JB03831.
0148-0227/97/96JB-03831$09.00

Tectonic Setting

Overview of the Geology of NW Thailand

Located in the triangle-shaped northern corner of Indochina (Figure 1a), NW Thailand is a mountainous region with moderate elevation (culminating at Doi Inthanon, 2576 m, D on Figure 1b) and rocks of various types and ages [*Baum et al.*, 1970; *Department of Mineral Resources*, 1982; *Hahn et al.*,

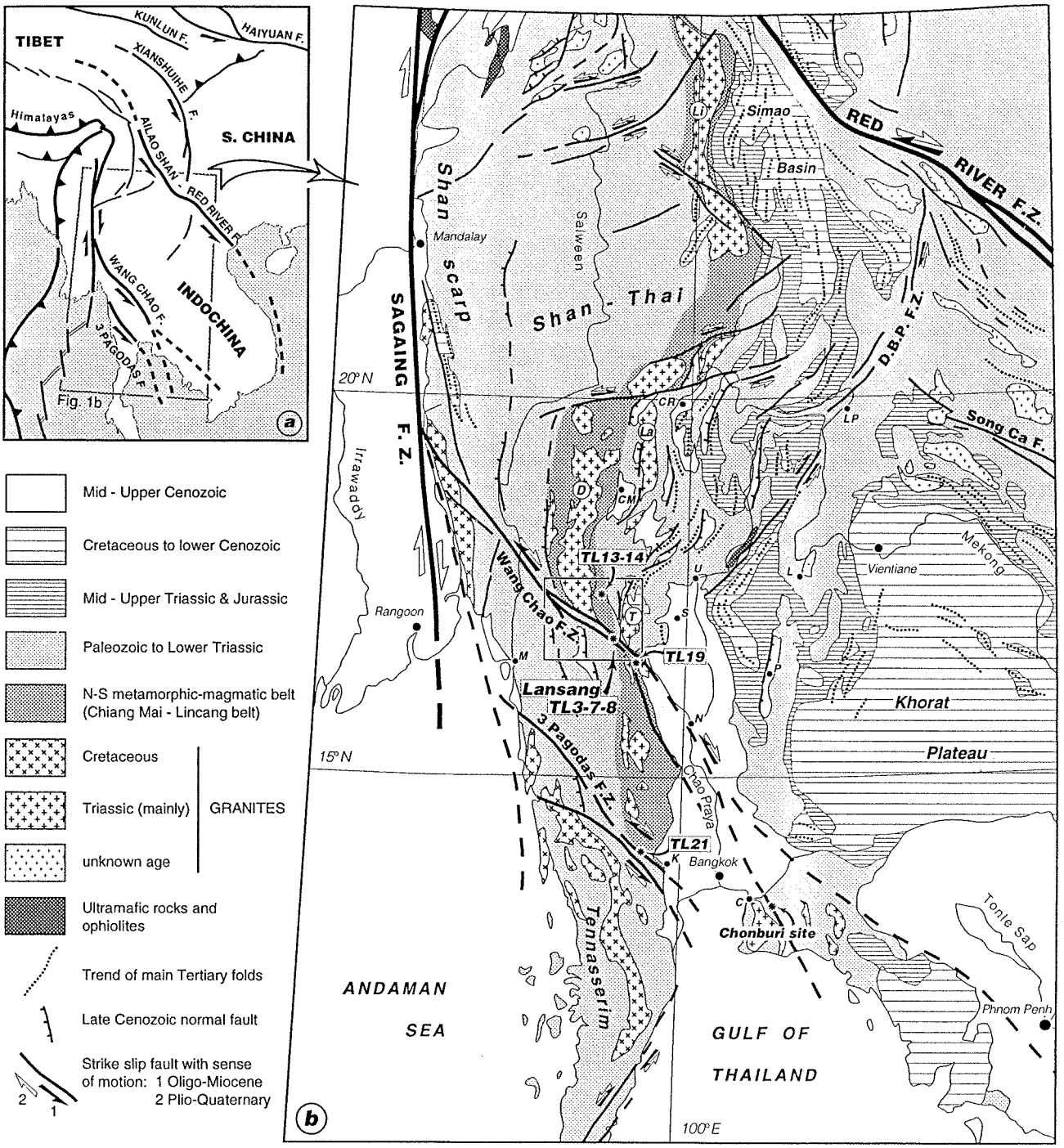

Figure 1. Structural and geological sketches of SE Asia showing location of studied areas in northwestern Thailand. (a) Map of major Cenozoic faults of mainland SE Asia and eastern Tibet [after *Leloup et al.*, 1995]. Arrows show senses of finite motion on strike–slip faults. Boxed area refers to Figure 1b. (b) Structural sketch map drawn from 1:5,000,000 scale geological map of Asia [*Department of Mineral Resources*, 1982], Landsat and Spot satellite images, ONC (Operational Navigation Chart) and TPC (Tactical Pilot Chart) topographic maps. Geological offsets (solid arrows) are inferred to have occurred coevally with Tertiary extrusion of Indochina [*Tapponnier et al.*, 1986, 1990a; *Leloup et al.*, 1995]. Present–day senses of motion (open arrows), deduced from morphological offsets and seismicity, are opposite to finite geological offsets [*Le Dain et al.*, 1984]. Trends of main Tertiary folds (dotted lines) are deduced from geological maps and satellite imagery. TL3-7-8, TL13-14, TL19, and TL21 refer to samples dated using $^{40}Ar/^{39}Ar$ ttechnique (see also Figure 2). DBPFZ is Dien Bien Phu fault zone; Li, La, D, and T, Lincang, Lampang, Doi Inthanon, and Tak metamorphic or magmatic massifs; U, Uttaradit; CM, Chiang Mai; CR, Chiang Rai; S, Sukhothai; N, Nakhon Sawan; K, Kanchanaburi; C, Chonburi; L, Loei; P, Petchabun; M, Moulmein; LP, Luang Prabang. Boxed area refers to Figure 2.

1986]. It lies ≈1500 km south of the eastern Himalayan syntaxis and 200 km east of the dextral Sagaing fault (Figure 1), present-day strike-slip boundary between India and Indochina.

The most prominent structural feature of the region is the Chiang Mai–Lincang belt (CM–L belt), a north-south, ≈70 km wide anticlinorium of metamorphic and magmatic rocks (Figure 1b). Toward the north, this belt forms the western border of the folded, Mesozoic Simao basin (Figure 1b), while south of the Gulf of Thailand it continues as the "main range batholith" along the Thailand–Malaysia border [*Hutchinson*, 1989]. This belt is offset by several strike-slip faults, the most prominent ones being the left-lateral Wang Chao and Three Pagodas fault zones (Figure 1b). The metamorphic rocks are mostly high-grade paragneisses, orthogneisses and micaschists. As they are locally overlain by less-metamorphic Paleozoic rocks, a Precambrian age has been ascribed to the gneisses and micaschists [*Baum et al.*, 1970; *Bunopas*, 1981; *Department of Mineral Resources*, 1982; *Hahn et al.*, 1986]. Contacts are generally faulted, however, and there is little evidence of stratigraphic conformity of the Paleozoic onto the gneisses [*Bunopas*, 1981; *Hahn et al.*, 1986]. The high-grade metamorphic rocks pass to deformed migmatites and are intruded by granitic plutons of mainly Permo–Triassic age [*Braun et al.*, 1976; *Beckinsale et al.*, 1979; *Hahn et al.*, 1986]. According to *Cobbing et al.* [1992], syntectonic migmatization and granite intrusion correspond to two successive stages of the same event, pointing to a Permo–Triassic age, rather than Precambrian, for the high-grade metamorphism. Younger magmatic and metamorphic events are suggested by radiochronologic studies and by the presence of Cretaceous or Tertiary granites in the CM–L belt [*Cobbing et al.*, 1992; *Dunning et al.*, 1995]. Larger Cretaceous to Paleogene granite plutons [*Beckinsale et al.*, 1979; *Hutchinson*, 1989; *Cobbing et al.*, 1992], offset left-laterally by the Three Pagodas fault zone [*Tapponnier et al.*, 1986], are found west of the belt from western peninsular Thailand in the south to the Tenasserim mountains of southern Burma and perhaps along the Shan scarp region (Figure 1b).

East of the CM–L belt, other large Triassic granite plutons have intruded the low-grade Paleozoic rocks of the Sukhothai fold belt [*Department of Mineral Resources*, 1982; *Hahn et al.*, 1986], between Sukhothai and Chiang Rai (S and CR, respectively, on Figure 1b). Apart from a broad antiform of Siluro–Devonian rocks east of Chiang Mai (CM on Figure 1b), the Sukhothai belt is chiefly made of upper Paleozoic to Mesozoic series (Carboniferous–Permian; Lower–Middle Triassic; Upper Triassic to Jurassic, separated by unconformiies) of sedimentary, volcanic and volcaniclastic (rhyolitic and andesitic) rocks [*Bunopas*, 1981; *Department of Mineral Resources*, 1982; *Hahn et al.*, 1986]. The latter Jurassic red bed series represents the southern extension of the Mesozoic to lower Cenozoic series of SW Yunnan (Figure 1b). Likewise, most of the folds of the Sukhothai belt (Figure 1b) prolongate those of the Simao basin where they are clearly due to Tertiary, ENE–WSW compression [*Tapponnier et al.*, 1990a]. Across NW Thailand, the N–S trending fold axes are bent into an S shape along the strike-slip faults north of Chiang Rai (Figure 1b). The folds are generally upright, though eastward to southeastward verging folds are reported along the borders of the Sukhothai belt [*Hahn et al.*, 1986]. Late Cenozoic grabens are localized along synclines of this former fold belt (Figure 1b). The sharp morphology of some of the ≈N–S normal faults that bound these grabens suggests that they are active. This tectonic style resembles that of Yunnan where active ≈E–W extension [*Tapponnier and Molnar*, 1977; *Allen et al.*, 1984] overprints the earlier Tertiary ENE–WSW compressional structures with mid-Tertiary thrusts reactivated as Plio–Quaternary normal faults [*Tapponnier et al.*, 1990a; *Leloup et al.*, 1995]. N–S grabens also exist below the central Thailand depression, beneath Quaternary sediments and in the Gulf of Thailand [*Polachan et al.*, 1991].

The Sukhothai fold belt is bounded to the east by the right-lateral Dien Bien Phu fault zone [*Tapponnier et al.*, 1986], whose trace is composed of several segments (Figure 1b). Some of the segments are presently reactivated in a "reversed," left-lateral sense. NE of Uttaradit (U on Figure 1b), a belt of ultramafic and mafic rocks, associated with basaltic to andesitic metavolcanics, blueschists [*Barr and Mac Donald*, 1987] and turbidites, stretches parallel to the Dien Bien Phu fault zone (Figure 1b). This belt marks the suture zone between the eastern, active margin of the Shan–Thai block, formerly the Sukhothai belt, and the passive margin of the Kontum–Khorat block to the SE [*Bunopas*, 1981; *Barr and Mac Donald*, 1987]. Subduction and subsequent collision probably occurred between the Upper Permian and the Middle Triassic [*Bunopas*, 1981; *Sengör and Hsü*, 1984; *Barr and Mac Donald*, 1987; *Hutchinson*, 1989]. East of this suture zone, the Loei fold belt (L on Figure 1b), affected by strong Triassic (Indosinian) folding, also displays pre–Upper Devonian deformation and metamorphism and may follow a Paleozoic suture zone [*Hahn et al.*, 1986]. Farther SE, post–Early Triassic folds and thrusts are clear on seismic profiles of the Khorat plateau (Figure 1b) where they are unconformably capped by the more gently folded, Mesozoic to lower Cenozoic, Khorat red bed series [e.g., *Mouret*, 1994].

Previous Geochronological Studies in NW Thailand

Most of the geochronological studies performed in Thailand have been focused on dating the various granitoids using Rb–Sr whole rock isochrons, or K–Ar dating of minerals [*Hahn et al.*, 1986]. Some of the published Rb–Sr ages [e.g., *Braun et al.*, 1976] are based on limited data sets, hence questionable [*Beckinsale et al.*, 1979]. Furthermore, K–Ar dating on minerals is inadequate to unravel complex thermal histories and may not date intrusion [*Beckinsale et al.*, 1979].

Granitoids in the Chiang Mai–Lincang and Sukhothai belts have yielded Triassic ages ranging mainly between ≈240 Ma and ≈200 Ma [e.g., *Braun et al.*, 1976; *Beckinsale et al.*, 1979; *Hahn et al.*, 1986; *Cobbing et al.*, 1992]. For instance, the Tak granodioritic to syenogranitic [*Mahawat et al.*, 1990] batholith (T on Figure 1b) gave Rb–Sr ages between 208 ±4 and 219 ±12 Ma [*Beckinsale et al.*, 1979; *Hahn et al.*, 1986]. The ages of the Lampang granite (La on Figure 1b) fall in the same range (212 ±12 Ma [*Beckinsale et al.*, 1979]). Toward the north, the Lincang batholith (Li on Figure 1b), yielded an older age with a large uncertainty (270 ±59 Ma, Rb–Sr [*Liu Changshi et al.*, 1989]). South of the Gulf of Thailand, in the Main Range batholith, U–Pb zircon dating (220 Ma to 198 Ma) confirms the Triassic age of the N–S magmatic belt [*Liew and Page*, 1985; *Hutchinson*, 1989].

Reliable geochronological results on metamorphic rocks are sparse. One U–Pb zircon discordia from a sample of the Lansang gneisses (Tak–Mae Sot section, Figures 2 and 3)

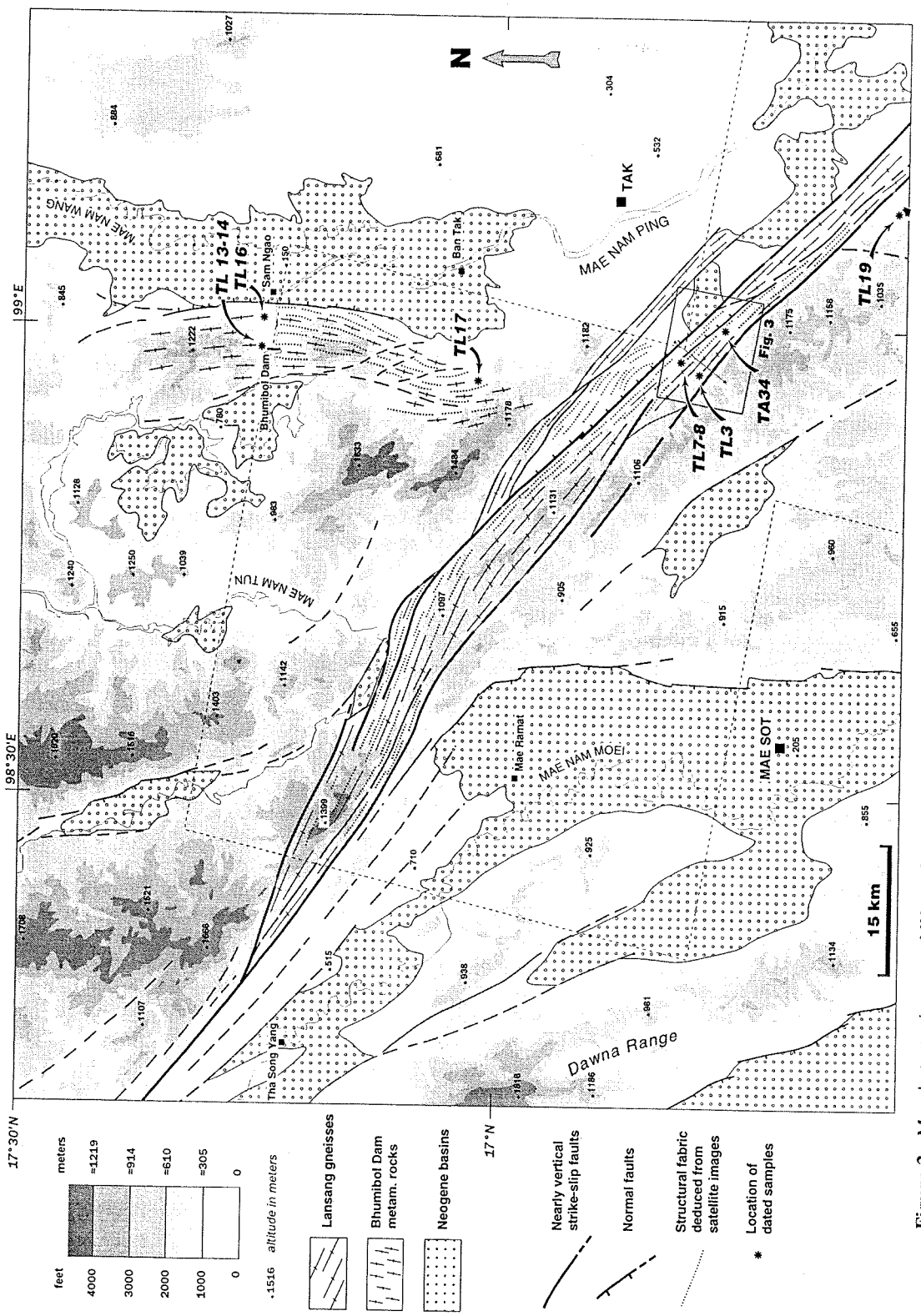

Figure 2. Morphotectonic map of Wang Chao fault zone in Tak–Mae Sot region. Faults and sketched geological overlay drawn from analysis of SPOT images, topography, 1:250,000 scale geological maps of Thailand [*Bunopas*, 1974; *Piyasin*, 1974; *Braun et al.*, 1981; *Sukto et al.*, 1984] and geological map of Burma [*Earth Sciences Research Division*, 1977]. Faults shown as continuous lines generally present characters of active faults (sharp morphological trace, topographic offsets). Highly elongated crosses correspond to mylonitic Lansang gneisses (Wang Chao shear zone); less elongated crosses show Bhumibol dam gneisses and schists. Structural trends (dotted lines), drawn from SPOT images, correspond to foliation and bedding planes. Topography from TPC-J10C 1:500,000 map. Dashed frame shows area covered by SPOT images used for mapping (KJ 257-316 and 258-317 of January 18, 1989). Boxed area refers to Figure 3. TL3, TL7-8, TA34, TL13-14, TL16, TL17, and TL19 show location of dated samples.

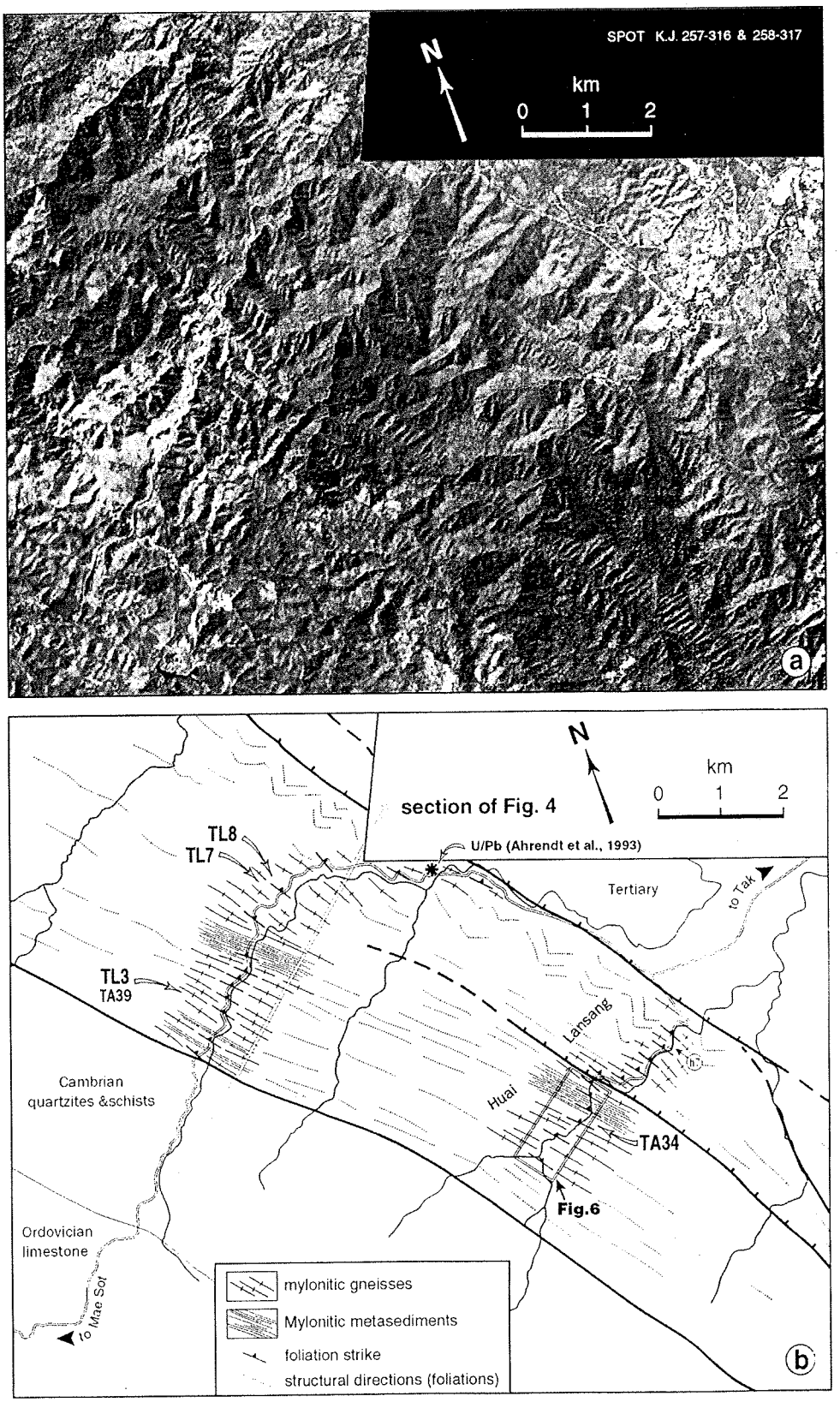

Figure 3. (a) Part of Spot K.J. 257-316 and 258-317 images showing Lansang park and Tak–Mae Sot highway area. (b) Geological interpretation drawn from SPOT images and map of *Campbell* [1973]. Lansang mylonitic gneisses are in grey. Foliation trends drawn from field measurements and SPOT images. Location of dated samples (TL3, 7, 8, TA34) and approximate location of U/Pb dated sample from *Ahrendt et al.* [1993] are shown. TA39 refers to sample of figure 8d. Site h7 along Huai Lansang corresponds to site of strain measurements of *Lacassin et al.* [1993].

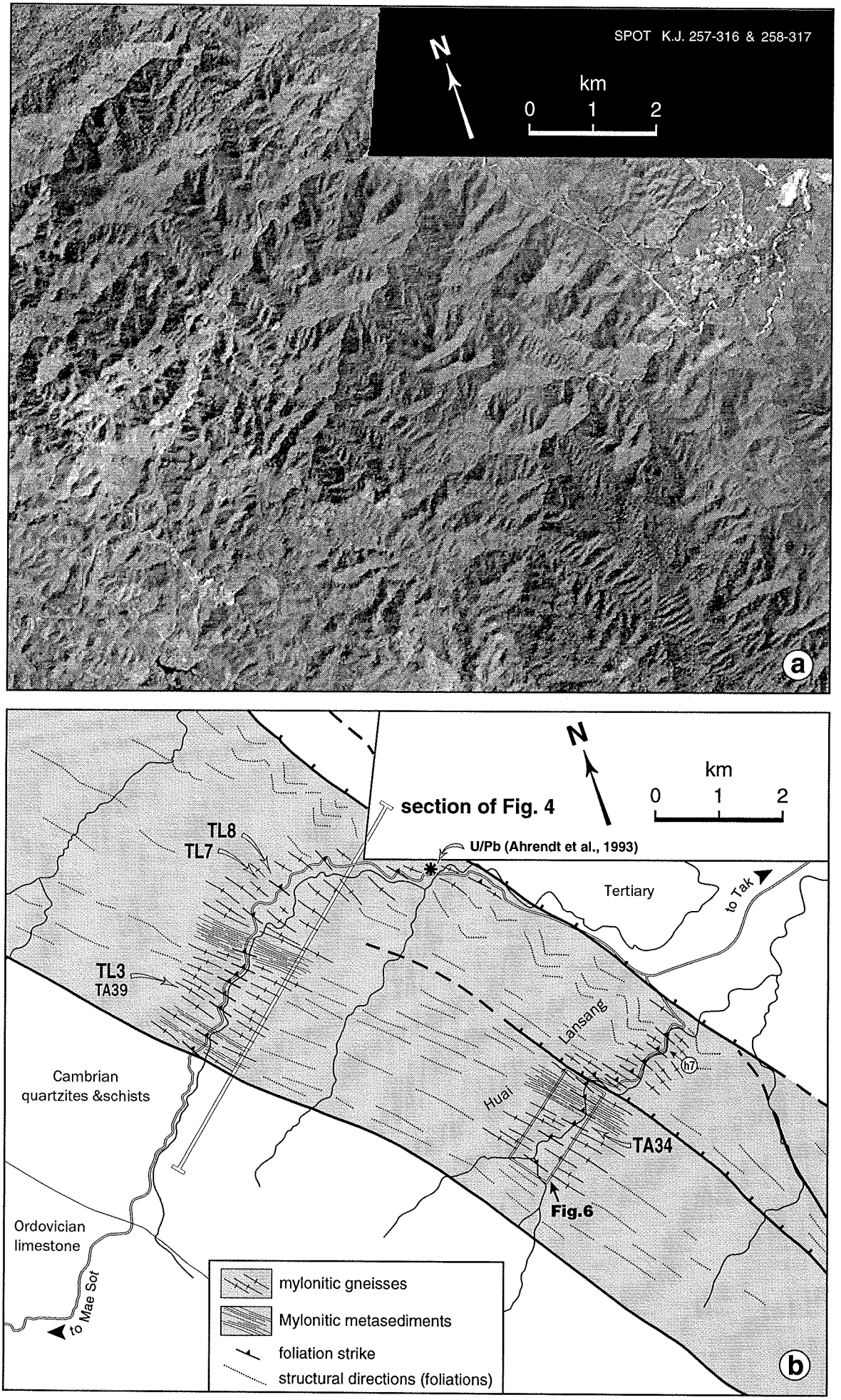

Figure 3. (a) Part of Spot K.J. 257-316 and 258-317 images showing Lansang park and Tak–Mae Sot highway area. (b) Geological interpretation drawn from SPOT images and map of Campbell [1973]. Lansang mylonitic gneisses are in grey. Foliation trends drawn from field measurements and SPOT images. Location of dated samples (TL3, 7, 8, TA34) and approximate location of U/Pb dated sample from *Ahrendt et al. [1993]* are shown. TA39 refers to sample of figure 8d. Site h7 along Huai Lansang corresponds to site of strain measurements of *Lacassin et al. [1993].*

gave an imprecise lower intercept age around 200 Ma [*Ahrendt et al.*, 1993]. K–Ar ages on biotites and illites from these gneisses (31.9 Ma to 29.6 Ma) are interpreted to result from Tertiary cooling [*Ahrendt et al.*, 1993]. Other Tertiary K–Ar ages on biotites and muscovites (27 to 29 Ma) are reported from the eastern border of the Chiang Mai–Lincang belt at the Bhumibol dam (Figure 2) and farther north near Hot and Chiang Mai (18 to 22 Ma) [*Braun et al.*, 1976; *Ahrendt et al.*, 1993]. In the region west of Chiang Mai, U–Pb dating of orthogneisses from the Doi Inthanon range (D on Figure 1b) yielded zircon lower intercept ages between 211 and 203 Ma, representing the age of the granitic intrusion [*Dunning et al.*, 1995]. Monazites gave nearly concordant U–Pb ages of 84 ±2 Ma and 72 ±1 Ma, interpreted as the age of the high-grade metamorphism [*Dunning et al.*, 1995]. The Mae Klang granite, which intrudes the eastern border of these gneisses, yielded concordant monazite and zircon results with an age of 26.8 ±0.5 Ma [*Dunning et al.*, 1995]. This latter granite is interpreted to have been emplaced during Oligo–Miocene low-angle normal faulting concurrent with the uplift of the high-grade gneisses [*Mac Donald et al.*, 1993; *Dunning et al.*, 1995]. More to the south the Thabsila gneisses [*Bunopas*, 1981] that form fault-bounded slivers within the Three Pagodas fault zone, yielded Rb–Sr ages of 391 Ma and 560 Ma at two different locations [*Bunopas*, 1981]. K–Ar dating of biotites from these gneisses, however, gave Tertiary ages of 36 ±1 Ma, 33 ±2 Ma [*Bunopas*, 1981]. These results suggest that the Chiang Mai–Lincang belt, site of Triassic granite emplacement, has suffered Upper Cretaceous and Tertiary deformation and metamorphic events whose importance and kinematics need to be assessed more precisely in many places.

Wang Chao, Three Pagodas Fault Zones and Adjacent Geological Units

The Wang Chao (also called Mae Ping or Papun) and Three Pagodas fault zones extend for about 450 and 250 km, respectively (Figure 1b). They probably continue toward the SE under the Chao Praya plain and in the Gulf of Thailand [*Bunopas*, 1981; *Tapponnier et al.*, 1986]. Both zones are composed of several strands striking NW–SE on average, roughly parallel to the Red River fault zone (Figure 1b). They cut and offset left-laterally the Chiang Mai–Lincang belt (Figure 1b), and distort the post Jurassic N–S trending fold axes [*Le Dain et al.*, 1984; *Tapponnier et al.*, 1986]. *Tapponnier et al.* [1986] and *Peltzer and Tapponnier* [1988] thus inferred that the total left-lateral offset (≈300 km) on these fault zones was a result of the Tertiary indentation of India within Asia. North of Chiang Mai, smaller conjugate dextral faults also offset the N–S metamorphic belt and bend the fold axes (Figure 1b). That segments of these faults are active is suggested by their sharp traces and the presence of river offsets on Landsat and SPOT images. The present-day slip senses deduced from such morphological offsets, however, are opposite to the finite geological offsets (Figure 1b). The way in which the ≈N–S trending Quaternary normal faults and grabens branch on these strike-slip faults (Figures 1b and 2), and fault plane solutions of earthquakes [*Le Dain et al.*, 1984] confirm the present-day slip senses. As in Yunnan, the upper Cenozoic deformation is thus compatible with E–W extension and N–S compression, perpendicular to the former mid-Cenozoic E–W shortening.

West of Kanchanaburi (K on Figure 1b), geological maps [*Bunopas*, 1976; *Department of Mineral Resources*, 1982; *Siribhakdi et al.*, 1985] show a 25 km wide zone of NW striking fault-bounded slivers parallel to the trend of the Three Pagodas fault zone (TPFZ). Most of these slivers are made of Permian or Triassic limestones, but metamorphic rocks (gneisses, quartzites, marbles) mapped as Precambrian (Thabsila gneisses) or lower Paleozoic [*Bunopas*, 1976] are exposed discontinuously in this zone. These metamorphic rocks generally show steep foliations and horizontal stretching lineations, both trending NW–SE parallel to the TPFZ. In some gneisses the lineation forms spectacular rods parallel to the fault zone. In this zone we sampled an orthogneiss to assess the age of metamorphism and deformation (Figure 1b).

Along the Wang Chao Fault zone (WCFZ), deformed rocks are exposed in the region of the Lansang National Park, SW of Tak (Figures 1b and 2). There a 5 to 8 km wide belt of mylonitic gneisses (Lansang gneisses) may be traced for about 130 km on geological maps and SPOT images (Figure 2). The fabric of the gneisses is clear on the images, everywhere nearly parallel to the boundaries of the gneiss belt and to the foliation and lithological banding observed on the outcrops (Figures 2 and 3). This belt is bounded to the SW by a steep fault zone with a sharp trace on SPOT images (Figures 2 and 3). Near the Lansang Park and for about 30 km northwestward, the rather steep northeastern range front, incised by small canyons, is marked by triangular facets (Figure 3). Such morphology implies recent uplift of the gneiss core by normal movement on the NE dipping fault that bound the gneisses to the NE (Figures 2 and 3). SPOT images show another NE dipping normal fault, also marked by triangular facets, within the gneisses (Figure 3). This fault limits to the NE the waterfalls of Huai Lansang, which are restricted to its footwall attesting for throw. South of the Mae Nam Tun valley (Figure 2), right-stepping fault segments, striking more easterly, form the northern boundary of the gneisses and cut across the mountain range. The Lansang gneiss core pinch out NE of Tha Song Yang (Figure 2). Still farther NW, the WCFZ is marked by parallel NW–SE striking faults, and by elongated hills of Triassic limestone along Mae Nam Moei river (Thai–Burma border). We have studied the deformation of the Lansang gneisses and mylonites along two sections SW of Tak (Lansang–Mae Sot road, Huai Lansang sections, Figure 3).

Lansang Mylonitic Gneisses

Earlier work: Petrography and general structure. The Lansang gneiss core is made of strongly deformed metasediments (quartz–feldspar–biotite (Q–F–Bi) paragneisses, micaschists, calcsilicate rocks, marbles), orthogneisses, and veins of pegmatite, quartz and microgranite [*Campbell*, 1973]. All these rocks dip steeply (≥45°) toward the northeast (Figure 4). The most frequent rocks are the Q–F–Bi gneisses, often migmatitic, that locally bear garnet, hornblende, and sillimanite [*Campbell*, 1976]. The calcsilicate rocks and marbles occur as bands of laminated mylonites parallel to the foliation and to the compositional layering of the surrounding gneisses (Figures 3, 4, and 5a). These rocks are interbanded with paragneisses and micaschists and with deformed pegmatite veins and orthogneisses (Figures 4 and 6). The close association of these rock types suggests a metasedimentary origin for the Q–F–Bi gneisses [*Campbell*, 1973]. The calcsilicate rocks, made of alternating green and purplish-brown bands, bear quartz, plagioclase, pyroxene, hornblende, calcite, ± muscovite and phlogopite, ± garnet [*Campbell*, 1976]. In these rocks, micro-

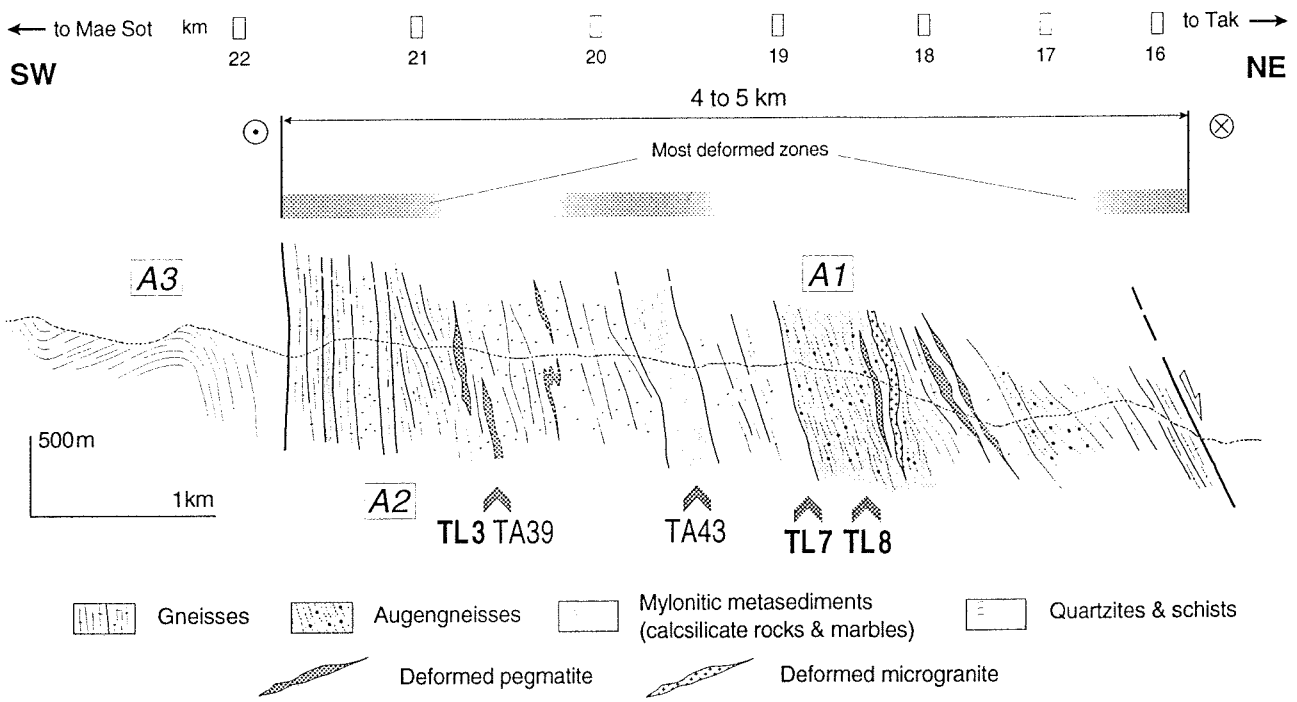

Figure 4. Geological section of Lansang mylonitic gneisses along Tak–Mae Sot highway (located on Figure 3b). Arrows labeled TL3, TL7, and TL8 locate dated samples. TA39 and TA43 correspond to samples of Figures 8d, and 8a, respectively. Sites of K–Ar dating of [*Ahrendt et al.*, 1993] are named A1, A2, and A3 (see text and Table 1). Most deformed zones are defined by prominent mylonitic textures, banding, and stretching lineations. On top, numbers 16 to 22 show approximate location of kilometer marker along road.

probe analyses (amphibole/plagioclase thermobarometry) yielded an estimate of 800 ±50°C for the high-grade metamorphism [*Martelet*, 1994]. The marble bands are made of a laminated dark gray rock bearing 90% of calcite (± quartz, feldspars, amphibole, phlogopite) [*Campbell*, 1976]. They contain up to 1 m wide boudins of calcsilicate rocks and of leucocratic granite (Figure 5f). A ≈500 m thick band of calcsilicate and marble rocks is found in the middle of the gneiss core along both the Tak–Mae Sot road and Huai Lansang sections (Figures 3b, 4, and 6). Metaigneous rocks comprise leucocratic gneisses and deformed pegmatite veins as well as granodioritic intrusions [*Campbell*, 1976]. Most are affected by penetrative deformation. According to Campbell, high-grade metamorphism, migmatization, and emplacement of leucocratic intrusions during the Precambrian would have been followed by intrusion of granodioritic rocks and by "postmetamorphic" mylonitization in the Paleozoic. The U–Pb age obtained by *Ahrendt et al.* [1993] on the gneisses possibly suggests, however, that high-grade metamorphism occurred around ≈200 Ma.

Characters of the ductile deformation. A major penetrative, ductile deformation, with steep foliations and nearly horizontal lineations (Figures 4, 5b, 6, and 7), affects all rock types of the Lansang gneisses. This deformation is particularly strong in the most deformable calcsilicate and marble band in the central part of the gneiss stripe (Figures 5a and 5d). On river-polished outcrops of Huai Lansang (site h4, Figure 6, for instance), they show clear macroscopic evidence of intense, nearly horizontal stretching and shear, including decimetric sheath folds, asymmetric boudinage with widely pulled-apart elements, meter-scale shear zones, rolling structures, and a prominent lineation (Figure 5b). Stretched garnets locally form thin elongated pink ribbons within these rocks. Under the microscope, the alternating white and darker bands of calcsilicate rocks appear extremely fine grained (Figure 8a). The finely laminated white bands, made of quartz and feldspar, bear stretched feldspar porphyroclasts commonly with elongated asymmetric tails. The darker bands are made of a fine-grained, calcitic matrix, embedding small rounded porphyroclasts of K-feldspar, plagioclase, hornblende, pyroxene, epidote, garnet and quartz of relatively homogeneous size (80 to 200 μm) (Figure 8a). The gray marbles present a similar microstructure with again a very small size of the calcite crystals within the matrix. This may suggest that grain boundary sliding or perhaps cataclastic shear has been a dominant deformation mechanism in these calcitic bands and that mylonitization has not been accompanied or followed by calcite recrystallization.

Most of the paragneisses, micaschists, and orthogneisses are mylonitic and show left-lateral shear bands (Figure 5e). The granitic and pegmatitic veins are generally as deformed as gneisses. Horizontal outcrops usually show these veins cut by shear planes and highly stretched [*Lacassin et al.*, 1993], while vertical sections perpendicular to lineation display folded veins (Figure 5c). Under the microscope, the gneisses generally bear biotite that outlines the foliation and the shear planes and marks the stretching lineation together with elongated ribbons of quartz and feldspars. Muscovite occurs as sheared asymmetric crystals (Figure 8c) and may form trails of pulled apart fragments. Quartz rich gneisses and micaschists often bear ribbons of elongated quartz crystals with a clear shape fabric oblique to the foliation and banding of the rock (Figure 8c).

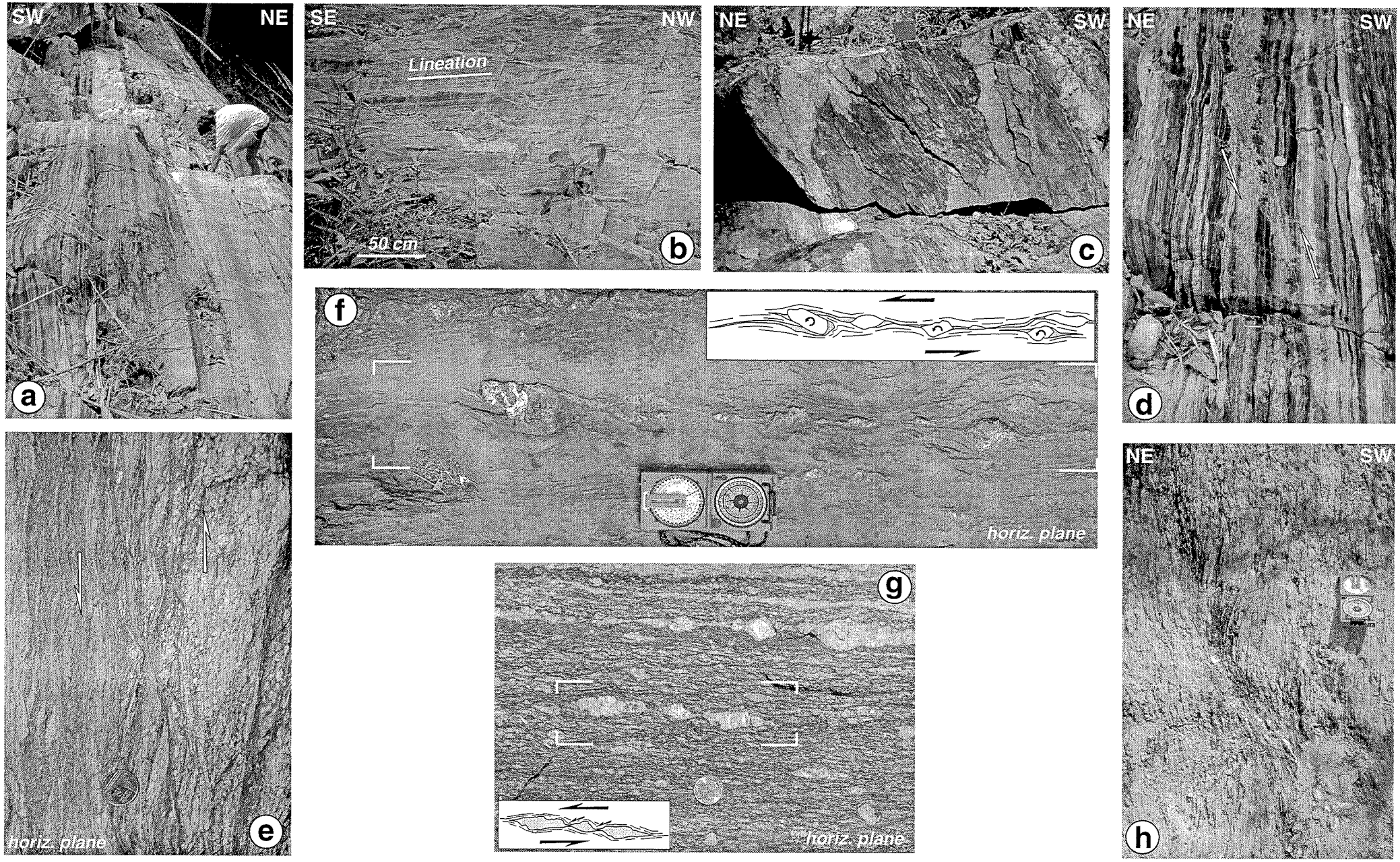

Figure 5. Characters of deformation in Lansang mylonitic gneisses. (a) Strong banding of rocks and steep foliation at site h4 (Figure 6). (b) nearly horizontal stretching lineation on steep foliation plane (site h4, Figure 6). (c) Folded pegmatitic vein on section perpendicular to lineation (site h3, Figure 6). (d) Brittle-ductile left-lateral shear zone at site h4 (Figure 6). (e) Left-lateral shear bands in gneisses from site h1 (Figure 6). (f) Rotated boudins affecting stretched leucocratic veins in dark-grey marble (site h6, Figure 6). (g) Asymmetric deformation of feldspar porphyroclasts in biotite bearing gneisses from sampling site TL8 (Figure 4). (h) Brittle-ductile left-lateral shear zone south of Nakhon Sawan (N on Figure 1b).

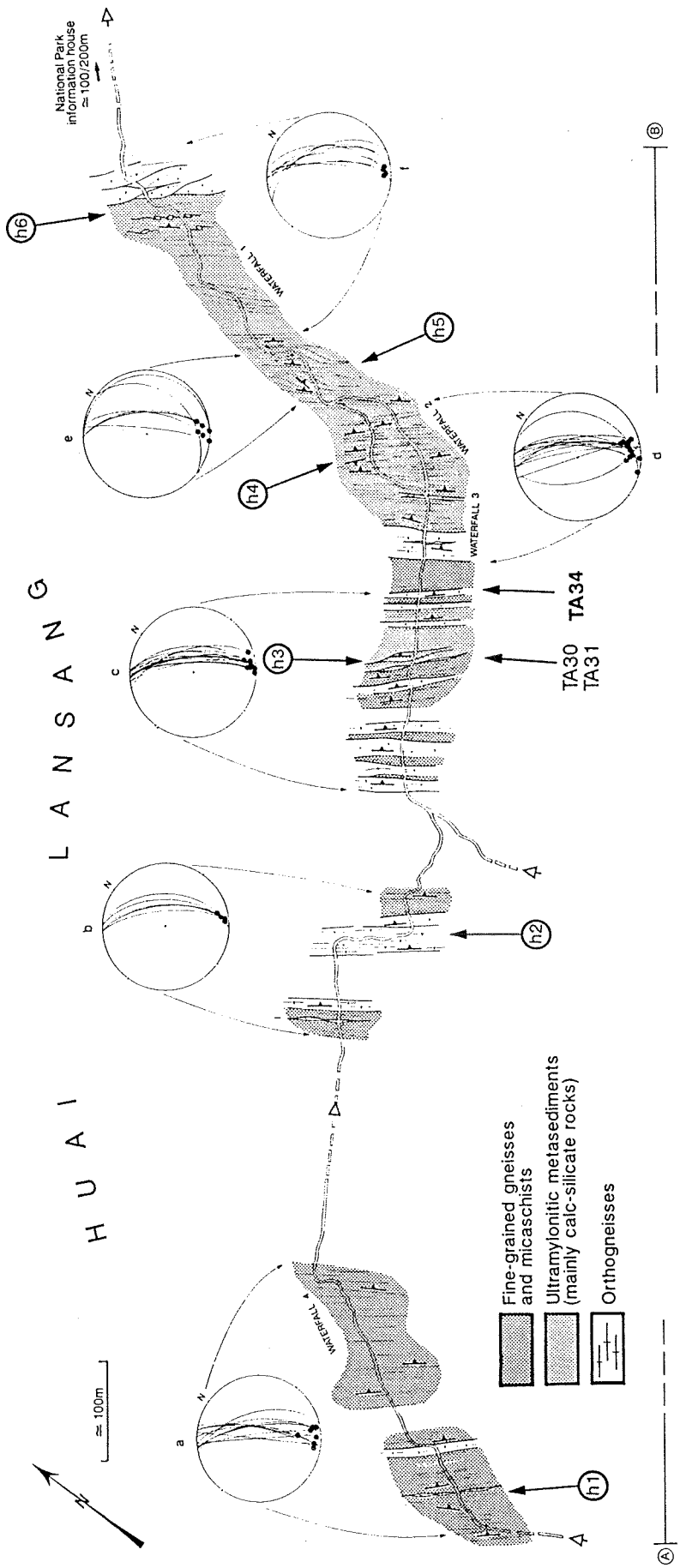

Figure 6. Map of central part of Lansang gneisses along Huai Lansang (boxed on Figure 3). Lower hemisphere Schmid diagrams show foliation and lineation attitude within six selected parts of section (labeled a to f). Markers h1 to h6 point to observation sites presented in text or figures. TA34 corresponds to dated sample (Figure 10). TA30 and TA31 locate samples whose microstructures are displayed on Figures 8b and 8c.

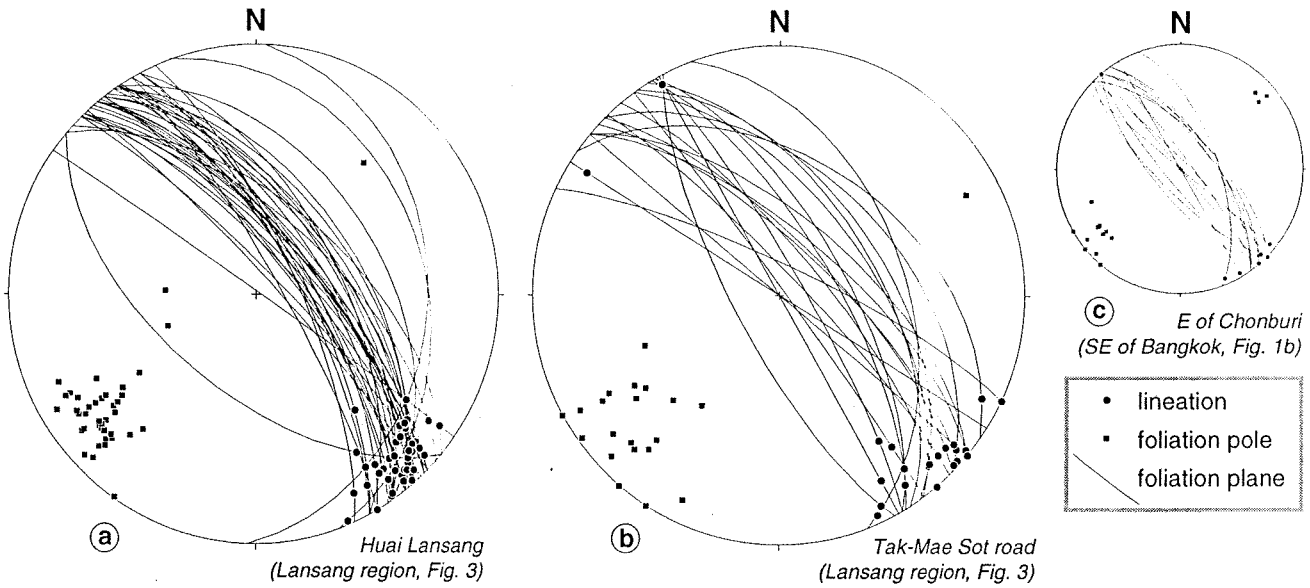

Figure 7. Measurements of foliation and lineation trends in Lansang mylonitic gneisses (Schmid net, lower hemisphere): (a) along Huai Lansang River and (b) along Tak–Mae Sot Road. (c) Lineation and foliations in probable southeastward extension of Wang Chao shear zone near Chonburi (Chonburi site on Figure 1b).

Close to the SW border of the gneisses, the banding of the rocks and the foliation planes are steep to nearly vertical (Figure 4). They flatten a little toward the NE and dip 45 to 60° NE in the NE half of the gneiss stripe (Figure 4). More gently dipping foliation planes are locally found where meter to 10 m scale folds fold the foliation. In spite of these variations in dip, the foliation planes always strike nearly parallel to the trend of the gneiss belt (Figures 3b, 6, 7a, and 7b) and bear everywhere a gently plunging stretching lineation (Figure 5b, 6, 7a, and 7b). Plunges of the lineation generally range between 0° and 20° toward the SE (Figure 6, 7a, and 7b).

Evidence for intense left-lateral shear. Clear shear sense indicators are found along Huai Lansang (Figure 6). There the detailed study of more than 25 river-polished surface outcrops yields systematic, left-lateral, macroscopic shear senses, confirmed by microstructural observations made on polished samples and under the microscope. Shear senses are deduced from various shear criteria [e.g., *Hanmer and Passchier*, 1991]. C/S and C'/S microstructures [*Berthé et al.*, 1979a, b] are common in gneisses (Figures 5e, 5g, and 8d), for instance, at sites h1, h2, h3, and h5 (Figure 6). Feldspar porphyroclasts are stretched, forming elongated, asymmetric tails commonly with well-developed rolling structures [*Van Den Driessche and Brun*, 1987; *Hanmer and Passchier*, 1991]. At site h6 (Figure 6), in marbles, stretched leucogranite or quartz veins form meter-scale rolling structures in which rotated boudin fragments are connected by elongated tails (Figure 5f). Asymmetric foliation boudinage also give consistent left-lateral shear sense [*Platt and Vissers*, 1980; *Gaudemer and Tapponnier*, 1987]. Under the microscope (Figure 8), shear senses are given by rolling structures, asymmetric boudinage of porphyroclasts, C or C' planes, deformed mica fishes [*Hanmer and Passchier*, 1991], and oblique shape fabrics of quartz [*Brunel*, 1980]. Along the Tak–Mae Sot road, determination of shear senses was more difficult in the field because of the lack of nearly horizontal outcrops, but the microstructural study of collected samples confirms the left-lateral shear sense.

The small-scale mylonitic banding of the rocks, the strong deformation of porphyroclasts, which are often elongated and exhibit long tails, the pervasive occurrence of asymmetric boudinage and C/S microstructures are qualitative indicators of the intensity of ductile strain. Decimetric sheath folds refolding the mylonitic foliation are found in the central calc-silicate band along both Huai Lansang (waterfalls 2 and 3, Figure 6) and Tak–Mae Sot road, together with folds parallel to the lineation (a folds). At site h5 along Huai Lansang (Figure 6), large-scale left-lateral foliation boudinage is combined with such folds, thus forming complex 3-D structures. Some of these structures refold already foliated marbles with boudins of mylonite, pegmatite, or quartz. Together with the widespread occurrence of mylonitic fabrics, the presence of sheath folds and a folds is consistent with intense progressive shear [*Cobbold and Quinquis*, 1980; *Lacassin and Mattauer*, 1985; *Malavieille*, 1987]. At the macroscopic scale the surface-balanced restoration of stretched veins from the northeastern part of the gneiss stripe (site h7, Figure 3) provides minimum estimates of the extension suffered by these veins (265 to 786%) [*Lacassin et al.*, 1993]. In the central calc-silicate bands, restoration of stretched porphyroclast using the same technique gave extension values of at least ≈450 to 865% [*Martelet*, 1994]. Assuming simple shear, these extension values imply lower bounds of 7 to 9 ±3 for the shear strain (γ) [*Lacassin et al.*, 1993; *Martelet*, 1994].

Nature of the Wang Chao–Lansang shear zone. The presence of widespread mylonitic fabrics with foliations, stretching lineations, and left-lateral shear criteria consistent from the microscopic to the regional scale imply that large sinistral shear occurred in the Lansang gneiss belt and led us to conclude that this belt is a major left-lateral ductile shear zone (the Wang Chao–Lansang shear zone). There is no clear evidence that would permit to infer that early shear increments have occurred in this zone under high-temperature conditions as in the Ailao Shan–Red River shear zone [*Leloup and Kienast*, 1993; *Leloup et al.*, 1995]. Indeed, the high-grade

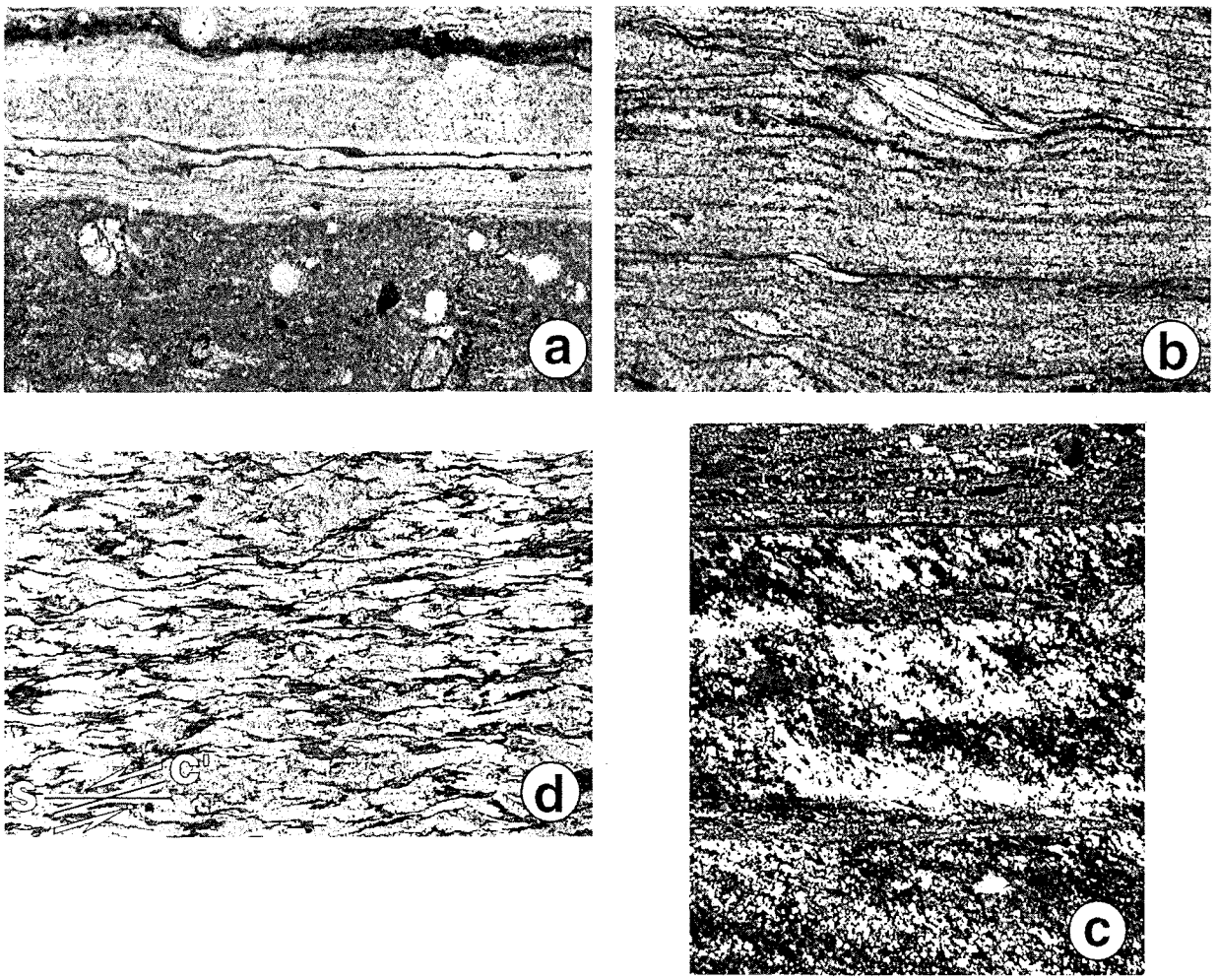

Figure 8. Microstructural characters of Lansang gneisses. (a) Mylonitic calcsilicate marbles (sample TA43, located on Figure 4). White quartzo–feldspathic ribbons alternate with darker bands made of fine–grained calcite matrix embedding rounded porphyroclasts (clinopyroxene, plagioclase, hornblende, K-feldspar, quartz, epidote). (b) Mylonitic paragneiss with sheared asymmetric muscovite crystals (sample TA30, located on Figure 6). (c) Mylonitic micaceous quartzite (sample TA31, located on Figure 6). Ribbons of recrystallized quartz grains with elongation oblique to ribbon edges and foliation. Sense of obliquity implies left–lateral shear. (d) C'/S gneisses (sample TA39, located on Figure 4) with left–lateral shear planes deforming biotite crystals.

assemblages are found in porphyroclasts (e.g., Figure 8a) and the pegmatitic and granitic veins are always deformed, suggesting that their emplacement predated most of the sinistral shear increments. On the other hand, progressive left–lateral shear clearly occurred under decreasing P/T conditions. Shear planes present various obliquities relative to foliation planes, ranging from nearly parallel to 20°–40° (Figure 5e, 5g, and 8d). The oblique shear planes generally strike more easterly (N120°E on the average) than the regional trend of the Lansang gneiss stripe, suggesting that they represent C' planes [*Berthé et al.*, 1979b]. Some of the latest brittle–ductile left–lateral shear planes contain chlorite. Brittle–ductile shear zones, with evidence of cataclasis at decimetric scale, also affect the calcsilicates and marbles (Figure 5d). In these rocks, more penetrative low–temperature deformation, with possibly cataclastic shear, might have occurred in the fine–grained ribbons embedding rounded porphyroclasts (Figure 8a). This body of evidence implies that progressive left–lateral shear, or at least late shear increments, occurred along a retrograde P/T path and were still ongoing at temperatures below the brittle–ductile transition in presently exposed rocks. Locally, in the northeastern part of the Lansang gneiss stripe, foliation planes bear chlorite–bearing down–dip slickensides due to normal, down to the NE, slip. Though minor compared to the ductile sinistral shear, these structures suggest that the gneisses have been brought to the surface by late normal faulting as for the Ailao Shan–Red River shear zone [e.g., *Leloup et al.*, 1995].

Chiang Mai–Lincang Belt Between the Lansang Area and Bhumibol Dam

To constrain the structure and age of the gneisses of the N–S metamorphic belt cut and offset by the WCFZ (Figure 1b), we sampled metamorphic rocks on either side of the Lansang gneisses, mostly where easily accessible, to the north (Figure 2). Between Sam Ngao and the Bhumibol dam, a ≈5 km long section cuts steeply dipping metamorphic rocks

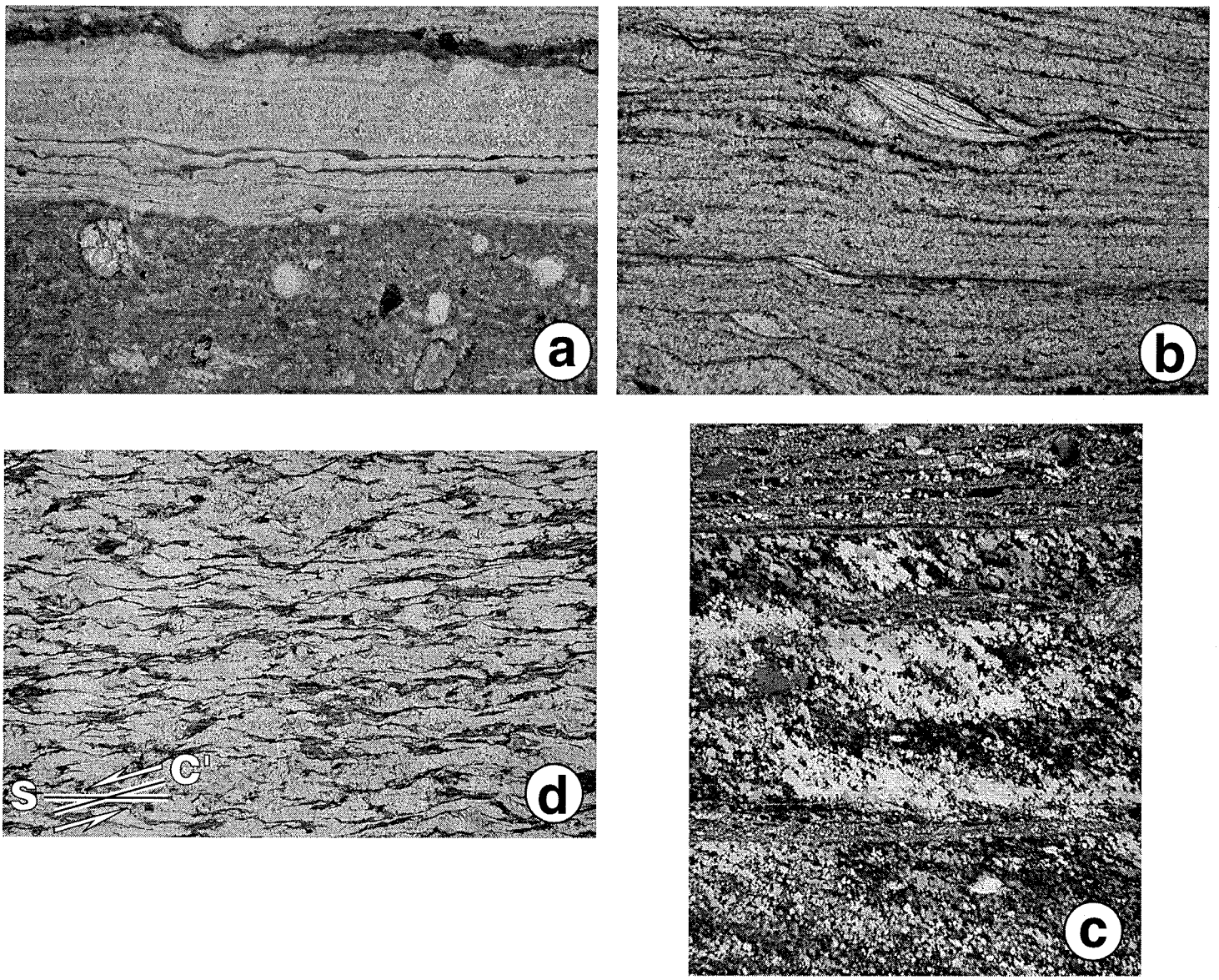

Figure 8. Microstructural characters of Lansang gneisses. (a) Mylonitic calcsilicate marbles (sample TA43, located on Figure 4). White quartzo–feldspathic ribbons alternate with darker bands made of fine–grained calcite matrix embedding rounded porphyroclasts (clinopyroxene, plagioclase, hornblende, K-feldspar, quartz, epidote). (b) Mylonitic paragneiss with sheared asymmetric muscovite crystals (sample TA30, located on Figure 6). (c) Mylonitic micaceous quartzite (sample TA31, located on Figure 6). Ribbons of recrystallized quartz grains with elongation oblique to ribbon edges and foliation. Sense of obliquity implies left–lateral shear. (d) C'/S gneisses (sample TA39, located on Figure 4) with left–lateral shear planes deforming biotite crystals.

(Yan He complex [*Bunopas*, 1981]) west of the late Cenozoic active Sam Ngao normal fault (Figure 2). Near the dam, the section exposes vertical schists, quartzites, quartz-bearing marbles, and rhyolitic to andesitic tufs with small feldspar porphyroclasts. These different rock types are finely intermixed, with 10 cm to 1 m scale banding. They display a vertical bedding parallel foliation ($S_{0/1}$) striking N175°E on the average. This foliation is strongly crenulated by folds with nearly horizontal axial planes, defining a N–S horizontal lineation. East of the dam series, one finds reddish schists (metapelites?) and a series of micaschists, metagreywackes, and quartzites. As at the dam, these rocks show steep bedding parallel cleavage affected by microfolds with N–S axes and a horizontal strain-slip cleavage (S_2) parallel to their axial planes. That micaschist sequence is bounded to the east by quartz-bearing marbles dipping steeply toward the east. The eastern part of the section is made of augengneisses, followed by low-grade schists and sandstones (Cambrian [*Bunopas*, 1981]), separated from the gneisses by a postmetamorphic fault. These moderately deformed gneisses form N–S striking rods with poorly defined foliation. Occasional garnet, sillimanite, andalusite, and cordierite are reported in the gneisses and micaschists [*Bunopas*, 1981]. Since we found no evidence of shear along this section, it seems probable that the rods in the gneisses, and the crenulation lineation in the quartzites, marbles, and schists mark fold axes rather than a strike-slip direction.

South of the dam section, west of Ban Tak, a large river bed outcrop also displays deformed metamorphic rocks (TL17 on Figure 2). The large-scale fabric, parallel to the $S_{0/1}$ foliation, may be followed in continuity from the dam section to this outcrop on the SPOT images (Figure 2), suggesting that both expose the same sequence. The eastern part of the outcrop is made of granite cut by nearly vertical brittle-ductile left-lateral shear zones and en échelon veins striking ≈N140°E, and N120°E, respectively. To the west, the granite intrudes a metasedimentary series made of alternating bands of grey to green quartzites, schists, marbles and calcsilicate bands bearing quartz, K-feldspar, plagioclase, pyroxene, carbonates, and ± garnet [*Martelet*, 1994]. Some bands bear large (1 to 10 cm) pink poecelitic garnets. In these rocks, the foliation strikes N–S on the average, dipping 70° toward the west, and bears a weak lineation plunging 40° to 60°S. The western part of the outcrop displays migmatitic gneisses and orthogneisses, with N10°E striking, vertical foliations, and lineation plunging ≈50°S. Deformed and undeformed veins of pegmatite and quartz intrude the metasediments and the gneisses.

The border of the Chiang Mai–Lincang belt thus displays different rock types (calcsilicates, marbles, quartzites and micaschists, migmatitic gneisses and orthogneisses intruded by pegmatitic and Quartz veins), mostly undeformed to moderately deformed. These lithologies resemble those found mylonitized within the Lansang gneisses. In particular, the green metasediments bearing large garnets found west of Ban Tak

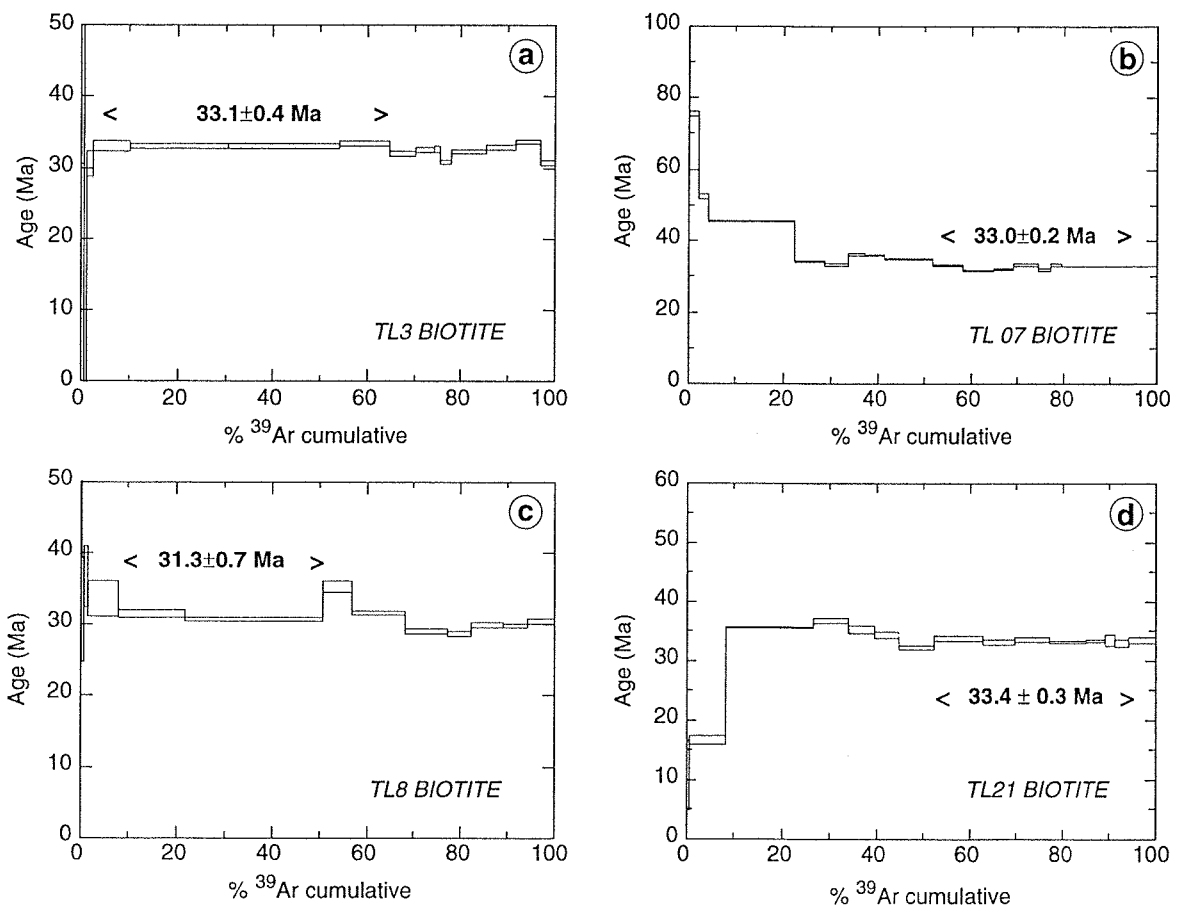

Figure 9. Results of $^{40}Ar/^{39}Ar$ biotite dating from Wang Chao shear zone (samples TL3, TL7, and TL8) and Three Pagodas fault (sample TL21). Samples located on Figures 2, 3b, 4, and 6.

could represent the parent rock type of the thinly banded green, grey, and brown mylonites of the central part of the Lansang gneiss stripe.

Age of Tectonometamorphic Events

We have dated metamorphic minerals from 11 samples of the Lansang mylonitic gneisses and other geological units nearby (located on Figures 1b, 2, and 3b) using the $^{40}Ar/^{39}Ar$ technique. The description of the dated samples and the factual presentation of the results and age spectra are given in the appendix. These results are graphically displayed on Figures 9 to 11 and summarized on Tables 1, 2, and 3. Analytical results are available on IPGP web site (http://www.ipgp.jussieu.fr/depts/tecto.html) or on request to the authors.

Early Oligocene Sinistral Shear Along the Wang Chao and Three Pagodas Faults

Biotites from the four samples of the Lansang gneisses yielded clustered results. Plateau ages, calculated for the flat part of the spectrum, are close to 33 Ma for TL3 and TL7, 31.3 Ma for TL8, and 30.6 Ma for TA34 (Figure 9 and Table 1). For TL3, TL8, and TA34, the total ages, calculated for the whole spectrum, are close to plateau ages (Table 1). Except for TL7, isochrons ages calculated from the inverse correlation plots are comparable, within uncertainties, to plateau ages, and $^{40}Ar/^{36}Ar$ ratio are close to the atmospheric ratio (Table 1).

Modelization of the TA34 K-feldspar spectrum assuming a discrete distribution of domain sizes for argon [*Harrison et al.*, 1991; *Lovera et al.*, 1991] provides a reasonable fit of the re-

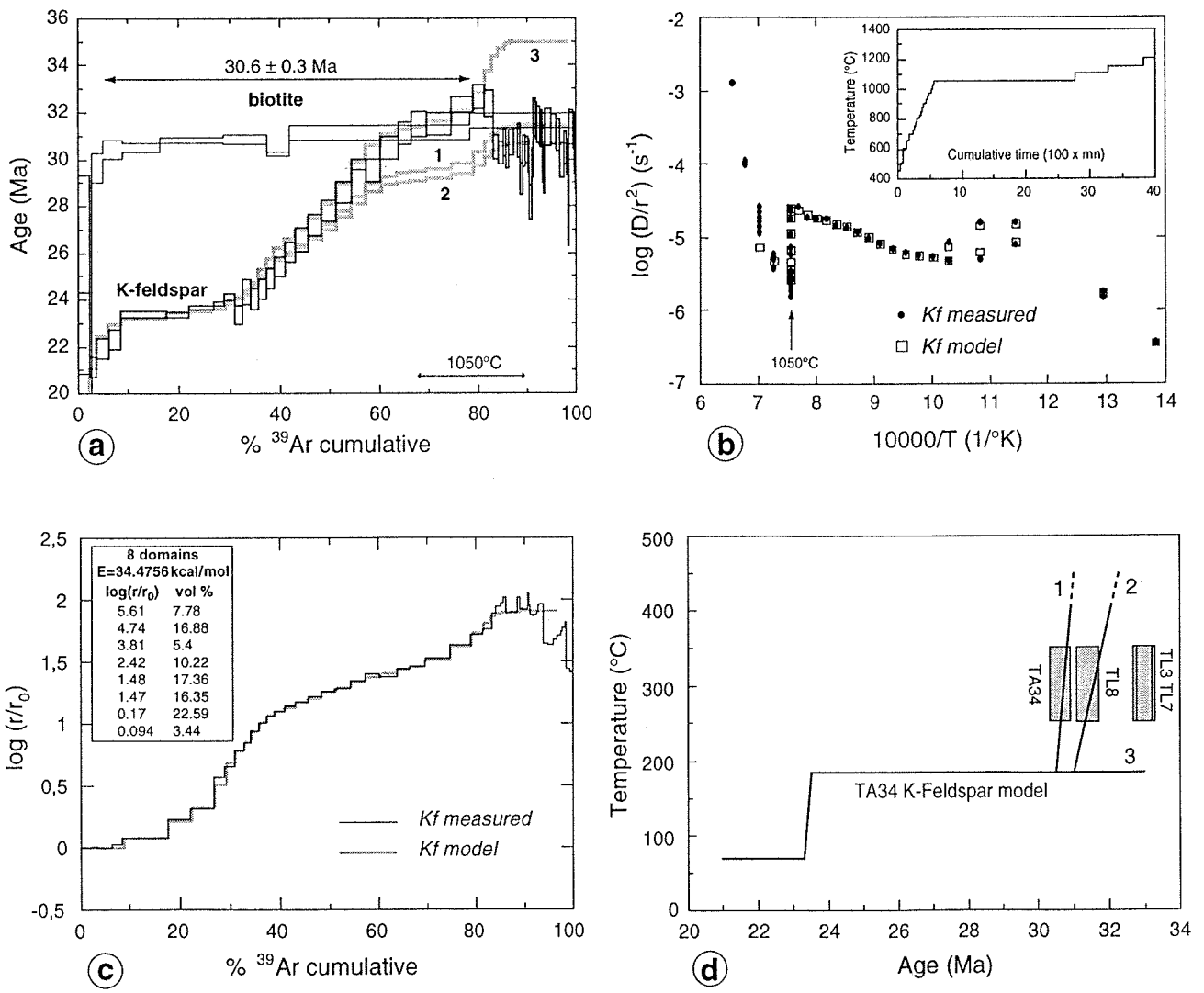

Figure 10. $^{40}Ar/^{39}Ar$ results obtained on TA34 sample (Wang Chao shear zone, located on Figure 3b and 6). (a) Age spectra of biotite and K-feldspar. Shaded curves show modeled K-feldspar age spectra for thermal histories 1 to 3 of Figure 10d. (b) and (c) Fit of model and data on the Arrhenius plot calculated from ^{39}Ar diffusivities (Figure 10b), and on the log (r/r_0) plot (Figure 10c). On Figure 10b and 10c, inserts show used thermal heating procedure and domain characteristics, respectively. (d) Thermal histories inferred from K-feldspar results. Solid lines show the three thermal histories discussed in text (fit to age spectrum is shown on Figure 10a). Only thermal histories 1 and 2 fit both K-feldspar and biotite results. Boxes show results of biotite dating (Tables 1 and 2) with closure temperature of biotite taken to be 300 ±50°C.

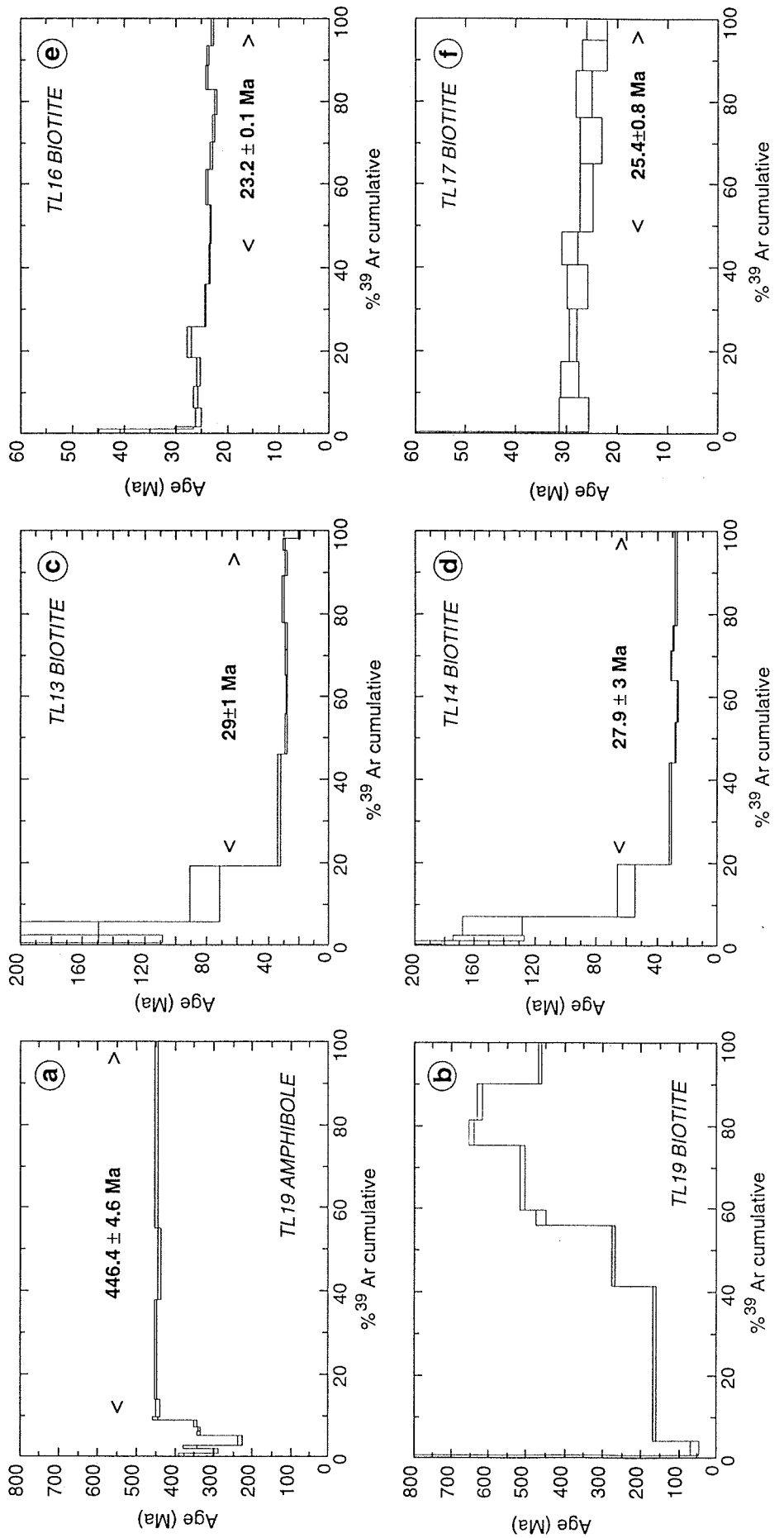

Figure 11. (a) and (b) Results of $^{40}Ar/^{39}Ar$ amphibole (Figure 11a) and biotite (Figure 11b) dating from gneisses southeast of Lansang mylonites (TL19 sample, located on Figures 1b and 2). (c) and (d) Results of $^{40}Ar/^{39}Ar$ biotite dating in metasediments from Bhumibol dam section, north of Lansang mylonites. Samples located on Figure 2. (e) and (f) Results of $^{40}Ar/^{39}Ar$ biotite dating in gneisses from Bhumibol dam section (Figure 11e, sample TL16) and outcrop west of Ban Tak (Figure 11f, sample TL17). Samples located on Figure 2.

Table 1. Results of $^{40}Ar/^{39}Ar$ Dating on Biotites and Amphibole

Sample	Plateau Age, Ma	Total Age, Ma	Isochron Age, Ma	$^{40}Ar/^{36}Ar$
TL3 biotite	33.1 ± 0.4	32.6 ± 0.4	33.0 ± 0.3	294 ± 5
TL7 biotite	33.0 ± 0.2	37.0 ± 0.2	(30.0 ± 0.5)	(1848 ± 50)
TL8 biotite	31.3 ± 0.7	31.2 ± 0,7	31.4 ± 0.3	288 ± 9
TA34 biotite	30.6 ± 0.3	30.5 ± 0.5	31.4 ± 1.8	286 ± 5
TL13 biotite	29 ± 1	46.2 ± 3.5	27.3 ± 0.6	324 ± 15
TL14 biotite	28 ± 3	44.6 ± 3	26.2 ± 1	344 ± 10
TL16 biotite	23.2 ± 0.1	24.3 ± 0.1	23.0 ± 0.6	335 ± 10
TL17 biotite	25.4 ± 0.8	28.1 ± 0.6	(27.2 ± 0.6)	(227 ± 12)
TL19 biotite		359 ± 6		
TL19 amphibole	464.4 ± 4.6	438.2 ± 3.5	450 ± 5	262 ± 10
TL21 biotite	33.4 ± 0.3	32.7 ± 0.8	(32.6 ± 0.5)	(320 ± 10)

Results for plateau ages are those retained for the age of the mineral. Values in parentheses are not significant (data clustering on isochron).

sults (Figure 10) for eight domains with a common activation energy of 35.5 kcal/mol. Such activation energy is quite low for K–feldspar (commonly 40 to 55 kcal/mol) but leads to a good fit to the experimental Arrhenius plot, except for the last 10% of Ar release (Figures 10b and 10c). Taking these domain characteristics (Figure 10c), theoretical age spectra [*Lovera et al.*, 1991] have been calculated for three possible cooling histories (Figures 10a and 10d). For cooling histories 1 and 2 (Figure 10d) we have not attempted to model the bump in the age spectrum, likely due to excess argon [*Foster et al.*, 1990]. This lead to modeled spectra shortcutting this bump (Figure 10a). These very similar thermal histories imply rapid cooling from ≈400°C to ≈185°C starting between 32.5 and 31 Ma (histories 2 and 1, respectively, Figure 10d) in order to fit the last 16% of Ar release (Figure 10a). After this rapid cooling and a first isothermal step (≈185°C), a second phase of cooling occurs at 23.5 Ma before the final isothermal step (≈75°C). Assuming closure temperature of 300 ±50°C for biotite, the age of TA34 biotite lie on, or is very close to, cooling curves 1 and 2 (Figure 10d). Note finally that an attempt to model the bump in the age spectra by neglecting the last 16% of degassing gave a cooling history unconstrained at high temperature and incompatible with biotite ages (curve 3, Figure 10d).

In view of the intense shear strain of the rocks, and of the retrograde character of the late deformation structures, we infer that the biotite ages obtained in the Lansang gneisses (33 and 30.6 Ma, Table 2) date the late stages of ductile left–lateral shear along the Lansang–Wang Chao fault zone. The thermal history deduced from TA34 K–feldspar dating and modeling supports this view (Figures 10 and 12). It shows that rapid cooling from ≈400°C down to 185°C, thus probably lower than the brittle–ductile transition, occurred around 31 Ma. This rapid cooling was probably coeval with the last increments of ductile left–lateral shear (Figure 12). The biotite of the same sample gives an age of 30.6 Ma in full agreement with the feldspar thermal history (Figure 10). The other samples give slightly different biotite ages (Table 1 and Figure 10d), suggesting that thermal histories and times of biotite closure for argon differed somewhat from place to place along section, or along strike in the gneisses, as in the Ailao Shan–Red River shear zone [*Harrison et al.*, 1992, 1996].

Table 2. Summary of Dating Results on the Wang Chao and Three Pagodas Fault Zones

Sample	Location	Mineral	Age, Ma	Tectonics
TL3	Lansang gneisses (Figures 3 and 4)	biotite	33.1 ±0.4	left–lateral shear
TL7	Lansang gneisses (Figures 3 and 4)	biotite	33.0 ±0.2	left–lateral shear
TL8	Lansang gneisses (Figures 3 and 4)	biotite	31.3 ±0.7	left–lateral shear
TA34	Lansang gneisses (Figures 3, 4 and 6)	biotite	30.6 ±0.3	left–lateral shear
		K–feldspar	rapid cooling at ≈30.5 Ma, 30 to 24 Ma: isothermal ≈185°C. rapid cooling at ≈23.5 Ma.	left–lateral shear cooling / uplift
Sites A1, A2, A3	Lansang gneisses (Figure 4) K-Ar [*Ahrendt et al.*, 1993]	K–Ar biotite (site A1) K–Ar illite (site A2) K–Ar illite (site A3)	29.9 ±0.6, 31.0 ±0.6, 31.9 ±1.6 29.6 ±1.2 30.5 ±1.0	Left–lateral shear Low T° Left–lateral shear Low T° Left–lateral shear
TL21	Three Pagodas fault (Figure 1)	biotite	33.4 ±0.4	left–lateral shear?
Thabsila gneisses	Three Pagodas fault K–Ar [*Bunopas*, 1981]	K–Ar biotite	36 ±1, 33 ±2	left–lateral shear?

Conventional K–Ar ages [*Ahrendt et al.*, 1993] on biotites from site A1 in the Lansang gneisses (Figure 4) range between 29.9 and 31.9 (Table 2) and are thus comparable to, or slightly younger than our $^{40}Ar/^{39}Ar$ results on TL7 and TL8 (33 ±0.5 Ma, 31.3 ±0.7 Ma). Some K–Ar ages on newly formed illite (29.6 ±1.2 and 30.5 ±1.0, at sites A2 and A3, respectively, Figure 4) also imply a low-temperature event around 30 Ma in these rocks [*Ahrendt et al.*, 1993].

A biotite age of 33.4 ±0.3 Ma has been obtained in the sample TL21 from the Three Pagodas fault zone (Figure 9d and Table 1). By analogy with the Lansang results, we interpret this age as the age of terminal left-lateral shear along that zone. This is also in line with the previous K/Ar dating results (36 ±1 Ma, 33 ±2 Ma, Table 2), possibly implying that shear lasted at least from 36 and 33 Ma B.P.

Evidence for Upper Oligocene Uplift

Several dated samples come from the N–S metamorphic series, smeared and offset within the Lansang shear zone (Figures 1b and 2). The existence, in the Chiang Mai–Lincang belt, of old basement rocks affected by a Paleozoic (≈446 Ma) metamorphic event is suggested by the age of TL19 amphibole (446 ± 5 Ma, Figure 11a and Table 1).

To our surprise, however, the four samples taken between the Bhumibol dam and the Lansang gneisses (TL13, TL14, TL16, TL17) did not yield old, Paleozoic or lower Mesozoic age. Instead, biotite ages from these samples range between 29 and 23 Ma (Figures 11c to 11e, Tables 1 and 3), broadly consistent with conventional K–Ar ages at the same localities [*Ahrendt et al.*, 1993]. As the dated rocks show no evidence of shear, these ages cannot be ascribed to a metamorphic–deformation event such as that in the Lansang gneisses. They rather indicate that, near Bhumibol dam, Tertiary cooling affected the rocks of the eastern border of the Chiang Mai–Lincang belt. Cooling of these rocks under the biotite closure temperature for Argon (300 ±50°C) was probably driven by uplift and denudation between 29 and 23 Ma. The ages from the western part of the Bhumibol section (TL13, TL14) are identical to (within uncertainties), or only slightly younger than, the ages of left-lateral shear in the Lansang gneisses (Tables 2 and 3). On the other hand, the orthogneisses of the eastern part of this section (TL16) and the gneisses west of Ban Tak (TL17) yield more recent, latest Oligocene ages (Table 3). Cooling of the rocks might have occurred at a different time or rate at the different sampling localities. Alternatively, the rocks may have followed a nearly isothermal temperature–time path, at the biotite closure temperature for Argon between 29 and 23 Ma (Figure 12). In this hypothesis the closure of biotite would have occurred at different times in the four dated samples depending on their chemical composition, on the effect of penetrative deformation, or of local thermal anomalies. Such scattering of biotite ages during a ≈300°C isothermal step is comparable to that documented in the Dian Cang Shan range of the Red River fault zone [*Leloup et al.*, 1993]. After this nearly isothermal step, rapid cooling would have occurred around 23.5 Ma (Figure 12), possibly driven by exhumation of the Bhumibol metamorphics along the Sam Ngao east dipping normal fault. The existence and the regional extent of this event is supported both by the TL16 biotite age and by the thermal history of the TA34 K-feldspar (Figures 10d and 12). Note, however, that only a few tens of kilometers east of the Bhumibol and Lansang sections the Tak granite yielded Mesozoic biotite K–Ar ages (215 ±10 Ma [*Braun et al.*, 1976; *Ahrendt et al.*, 1993]) suggesting that late Oligocene cooling was restricted to the ranges east of Tak.

Summary and Discussion

Oligocene Strike–Slip Shear Within Indochina

Our structural analysis and $^{40}Ar/^{39}Ar$ dating of metamorphic minerals show that ductile left-lateral shear occurred during the Oligocene along the Wang Chao fault zone. Such shear was localized mostly in the elongated, 5 km wide, mylonitic core of the Lansang gneisses. From 32.5 to 30.5 Ma, rapid cooling of the gneisses accompanied the late stages of left-lateral motion (Figure 12). Modeled TA34 K-feldspar thermal history (Figure 10d) implies that temperature had droped below 185°C at about 30.5 Ma, a level too low to permit the continuation of ductile shear. This does not preclude continuation of left-lateral brittle faulting for some time after 30.5 Ma, as suggested by the existence of left-lateral brittle shear zones within the mylonites. Along the Three Pagodas fault zone, 250 km farther south, a lowermost Oligocene age deformation (36 to 33 Ma), somewhat older than in the Lansang gneisses, is suggested by $^{40}Ar/^{39}Ar$ and K–Ar dating.

A lower bound of 35 to 45 km of left-lateral displacement by ductile shear on the Wang Chao fault zone may be deduced from the restoration of boudin trails in the Lansang gneisses (shear strain γ of 7 to 9 within a ≈5 km thick shear zone) [*Lacassin et al.*, 1993; *Martelet*, 1994]. The larger geological offsets visible on extant maps provide a better estimate of the total displacement [*Tapponnier et al.*, 1986]. Along the Wang Chao fault, both the Chiang Mai–Lincang belt and the westernmost occurrence of the Triassic granites are offset

Table 3. Summary of Dating Results From the N-S Metamorphic Belt on Sides of the Wang Chao Shear Zone

Sample	Location	Mineral	Age, Ma	Tectonics
TL19	South of Lansang gneisses (Figures 1 and 2)	amphibole biotite	446.4 ±4.6 supports Paleozoic age	high-grade metamorphism
TL13	Bhumibol dam (Figure 2)	biotite	29.0 ±1	cooling/uplift
TL14	Bhumibol dam (Figure 2)	biotite	28 ±3	cooling/uplift
TL16	Bhumibol dam (Figure 2)	biotite	23.2 ±0.1	cooling/uplift
TL17	West of Ban Tak (Figure 2)	biotite	25.4 ±0.8	cooling/uplift
	Bhumibol dam [*Ahrendt et al.*, 1993]	K–Ar biotite K–Ar muscovite	28.5 ±0.6 29.0 ±1.0, 27.0 ±0.8	cooling/uplift

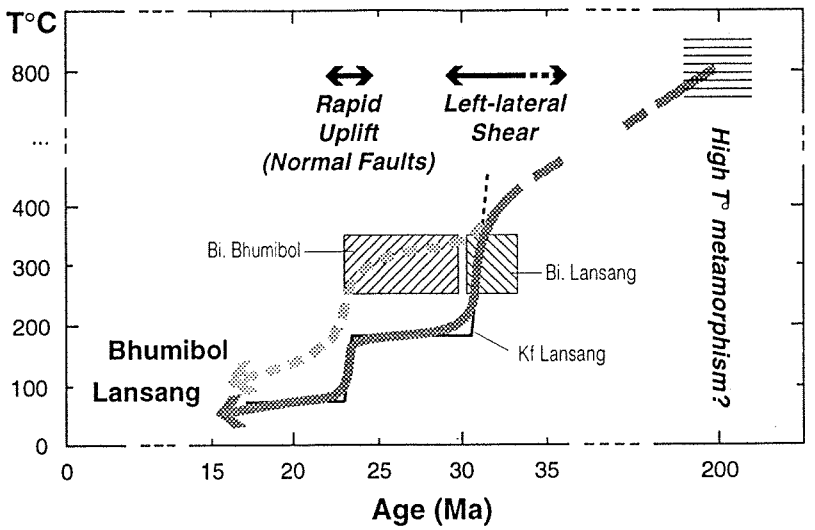

Figure 12. Time–temperature paths for Lansang mylonitic gneisses (dark gray) and for border of Lincang–Chiang Mai belt between Bhumibol dam and Lansang gneisses (light gray). Temperatures and ages deduced from biotite results (boxes with diagonal hatching) and K-feldspar modeling (solid line). Temperature conditions of high-temperature metamorphism from *Martelet* [1994]. Age of this metamorphism (≈200 Ma according to *Ahrendt et al.* [1993]) is poorly constrained.

by about 160 km (Figure 1b). A comparable offset has been estimated along the Three Pagodas fault zone by *Tapponnier et al.* [1986]. Such large offsets ought to result from long-lasting progressive shear. Indeed, at realistic plate tectonic rates (e.g., 1.5 to 3 cm/yr), 5 to 10 m.y. are required to produce a displacement of 150 km. We conclude that about 300 km [*Peltzer and Tapponnier*, 1988] of sinistral motion took place between approximately 40 Ma and 30 Ma along the Wang Chao–Three Pagodas (WCTP) fault system.

Such results bring strong support to the hypothesis that such left-lateral movements were an early consequence of the India–Asia collision [*Tapponnier et al.*, 1986; *Peltzer and Tapponnier*, 1988]. They imply that the southwestern part of Sundaland was extruded farther toward the SE in part earlier (Upper Eocene–Lower Oligocene) than the bulk of Indochina by left-lateral motion along the Ailao Shan–Red River shear zone (Figures 13b and 13c). Recall that motion along this latter zone, now firmly established between ≈26 and 17 Ma [*Schärer et al.*, 1994; *Leloup et al.*, 1995], may have started around 35 Ma [*Briais et al.*, 1993; *Schärer et al.*, 1994]. Rocks of the Lansang–Wang Chao shear zone suffered rapid cooling during late left-lateral shear (Figure 12), as observed in the Ailao Shan about 10 m.y. later [*Harrison et al.*, 1992; *Leloup et al.*, 1995; *Harrison et al.*, 1996]. The same exhumation mechanism invoked to explain uplift in the Ailao Shan, that is north dipping normal faulting during sinistral transtension, appears to have brought the Lansang gneisses to the surface. After cessation of left-lateral shear, the sense of motion along the WCTP fault system reversed to right lateral [*Le Dain et al.*, 1984]. Our study suggests that such inversion may have been coeval with the onset of E–W extension around 23.5 Ma.

Southeastward and Offshore Continuation of the Wang Chao and Three Pagodas Faults

Towards the SE the Lansang mylonitic core disappears below the upper Cenozoic deposits of the Chao Praya plain (Figure 1b). Near Nakhon Sawan (N, Figure 1b), roughly in line with this core, small outcrops of basements rocks display granitic rocks affected by vertical, N–S striking cleavage and brittle–ductile left-lateral shear zones parallel to the trend of the Wang Chao fault (Figure 5h). Farther SE a branch of that fault continues east of Chonburi (Chonburi site, Figure 1b) where high-grade mylonitic rocks with steep foliations, nearly horizontal NW trending stretching lineations (Figure 7c) and left-lateral shear indicators are found. Metamorphism and deformation of these rocks are undated. Given the amount of displacement, this branch of the Wang Chao fault, as those of the Three Pagodas fault zone may continue offshore in the Gulf of Thailand (Figure 1b). Another splay of the Wang Chao fault probably continues along the Tonle Sap depression of Cambodia and farther SE, to the west end of the Mekong basin [*Tapponnier et al.*, 1986]. Southeastward, all the main left-lateral fault zones of western Sundaland thus enter regions where extensional basins formed during the Cenozoic (Figure 13a). This led *Tapponnier et al.* [1986] and *Peltzer and Tapponnier.* [1988] to infer that sinistral movement on these faults induced rifting in these basins, just as motion on the Red River fault zone initiated rifting and drove seafloor spreading in the South China Sea [*Tapponnier et al.*, 1986; *Briais et al.*, 1993].

Subsidence and sedimentation in the basins that floor the Gulf of Thailand and the shallow seas between Malaysia, Borneo and southern Vietnam occurred mainly in the mid–upper Cenozoic [e.g., *ASEAN Council on Petroleum*, 1981; *Hutchinson*, 1989]. Table 4 summarizes published structural and stratigraphic data on these basins together with key references. In the Malay basin, the Mouth of Mekong basins, and parts of certain basins in the Gulf of Thailand, such as the deeper part of the Pattani trough (Figure 13a), rifting and rapid sedimentation were coeval with left-lateral motion along the WCTP fault system (Table 4). In addition to geometry, the timing of sedimentation in these basins is adequate for them to have opened as left-lateral pull-aparts at the termination of the left-lateral faults (Figures 13a to 13c) [*Tappon-*

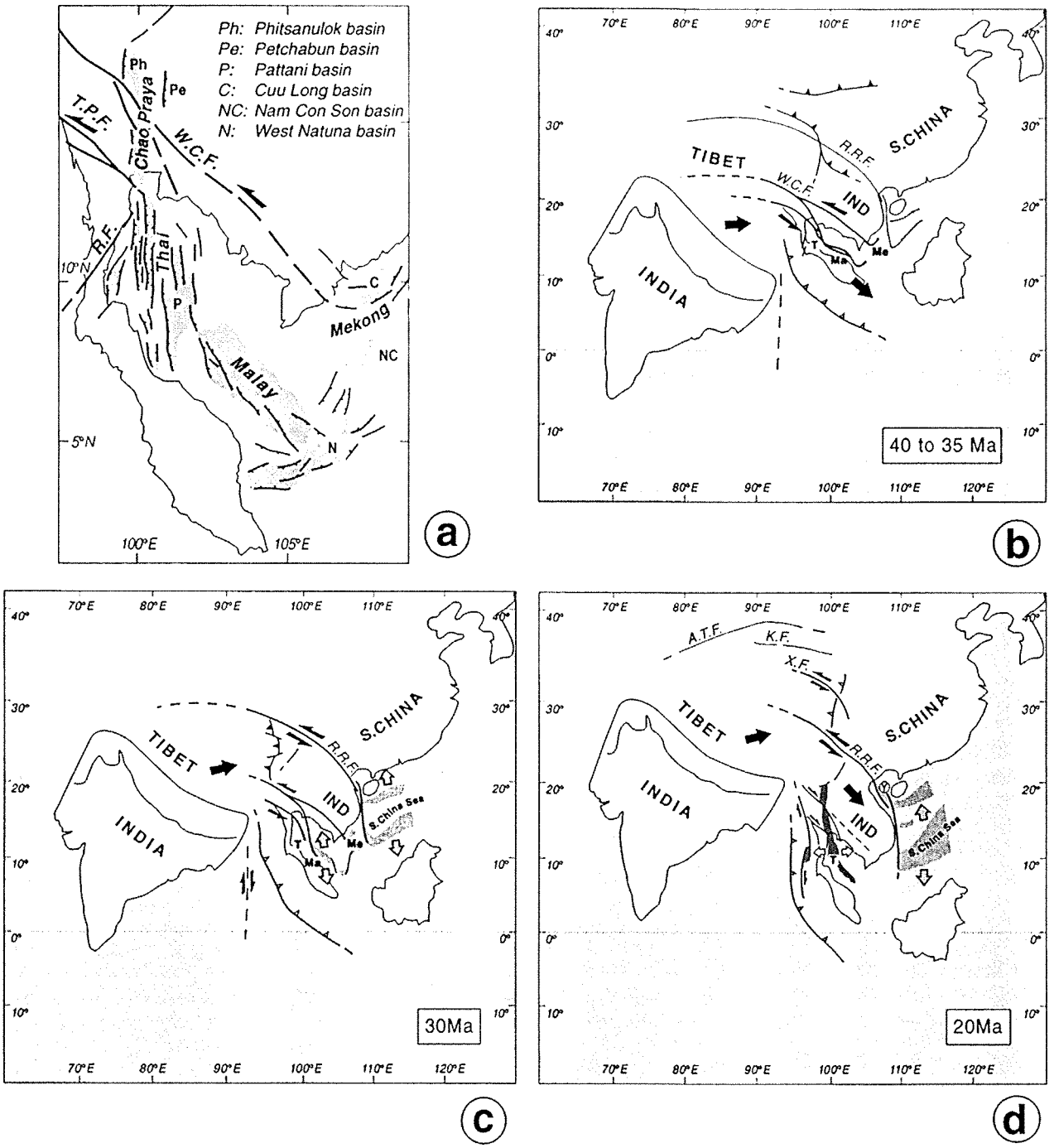

Figure 13. Speculative sketches of successive extrusion phases from late Eocene to lower Miocene, and relation with basin opening at southeastern tip of major faults. (a) Structural sketch of main Cenozoic basins after *ASEAN Council on Petroleum* [1981], *Hutchinson* [1989], and *Mai Thanh Tan* [1995]. W.C.F., T.P.F., R.F., Wang Chao, Three Pagodas, and Ranong faults, respectively. (b) Plate and continental block situation in upper Eocene (40 to 35 Ma). Begining of sinistral motion on Three Pagodas–Wang Chao fault zone (W.C.F.), extrusion of southwestern Indochina, and correlative opening of Malay (Ma), Mekong delta (Me), and parts of Gulf of Thailand (T) basins. (c) Lower Oligocene (≈30 Ma). Major extrusion of Indochina (IND), with sinistral motion along Red River Fault (R.R.F.), and opening of South China Sea. This occurred coevally with latest shear increments along Three Pagodas–Wang Chao fault zone. (d) Lower Miocene (≈20 Ma), sinistral motion continued along Red River fault together with opening of South China Sea and Yinghehai (Y) pull–apart basin [*Leloup et al.*, 1995]. In souwestern Indochina, onset of E-W extension in Gulf of Thailand (T) possibly driven by dextral reactivation of Three Pagodas–Wang Chao fault zone. X.F., K.F., A.T.F. are future traces of Late Cenozoic Xianshuihe, Kunlun, and Altyn Tagh sinistral faults, respectively. Motion of India relative to Asia is after *Patriat and Achache* [1984] and *Besse and Courtillot* [1988]. Poles and rotation rates for Indochinese blocks are those of *Briais et al.* [1993] adapted by *Leloup et al.* [1995].

Table 4. Summary of Stratigraphic and Structural Data on Cenozoic Basins of the Gulf of Thailand and Northern Thailand

Basin	Geometry	Depth, Older Sediments	Tectonic and Sedimentary Evolution
Malay basin (Malay or Ma on Figure 13)	NW-SE elongated deep trough[a, b, c] Strongly resembles Yinggehai basin (offshore extension of Red River fault)	Depth ≥10 000 m, mainly nonmarine sediments[a]. Deepest wells reached Oligo-Miocene at about 3000 m, lower part of section not known but inferred to be Eocene[b, c].	Extension and crustal stretching probably in early Tertiary[a] (Eocene to Oligocene). Then regional subsidence and sedimentary infilling (upper Oligocene, Miocene). Reportedly, "structural break" at the end of Oligocene[a]. Unconformity between mid-Miocene and Pliocene[a].
Gulf of Thailand basins (Thai on Figure 13a)	Mainly N-S grabens and half-grabens[a, b, c]. N–S structural trend possibly due to influence of older structures[a].	Up to 8000 m deep (eastern Pattani basin), shallower basins to the west[a]. Mainly nonmarine: offlap regressive sequences followed by late Miocene marine transgression. Drilled late Oligocene, still older rocks inferred in deepest parts[a, d, e].	Tectonic extension around 36 to 33 Ma in some parts of the basins[f]. Second phase of fault controlled subsidence around 22.5 Ma[f]. Late Miocene to Pliocene regional subsidence. Early Miocene reported to be unconformable on the Oligocene (?) conglomeratic series[a].
Chao Praya plain and Petchabun basin (Figure 13a)	N-S grabens and half-grabens[b, e, g].	Depth 2000/4000 m; 8000 m deep in Phitsanulok basin[d, e]. Late Oligocene to early Miocene lacustrine-fluviatile clays and sandstones[e, g].	Opening (E-W extension) in the upper Oligocene to early Miocene[b, e, g], followed by important clastic sedimentation and subsidence during the Miocene[b, e, g]. Recent and moderate Plio–Quaternary regional subsidence.
Intramontane basins (north of W.C.F., Figure 1)	N-S grabens and half–grabens[b, e].	Depth 1000 to 4000 m; stratigraphy poorly known[e], early Miocene mammals remains[h].	Miocene to recent E-W extension, in part related to strike–slip movements (Figure 1b). No significant regional subsidence.
Mekong delta basins (Cuu Long and Nam con Son basin, C and NC on Figure 13a, respectively)	Arcuate, mainly NE-SW trough[i].	Depth 6000 m in Mekong trough[i], 12 km in Nam Con Son basin[j]. Thick (3000 m) Upper Eocene to lower Oligocene series in middle of Mekong trough[b, i]. Below Mekong delta, small grabens (2000 to 4000 m deep), filled by upper Eocene coarse sediments[i].	Graben formation and localized subsidence in the upper Eocene and Oligocene[b, i, j] Regional subsidence in the middle Miocene to Plio–Quaternary[i, j, k]. Unconformities reported between Oligocene and Miocene [k], and in early middle Miocene[i, j].

Regional subsidence means that subsidence (probably thermally induced) and sedimentation occur over a wide region and generally blanket the previously formed localized grabens.

[a] *ASEAN Council on Petroleum* [1981].
[b] *Hutchinson* [1989].
[c] *Hamilton* [1979].
[d] *Bunopas and Vella* [1983].
[e] *Polachan et al.* [1991].
[f] *Pigott and Sattayarak* [1993].
[g] *Remus et al.* [1993].
[h] *Ducrocq* [1992] and *Ducrocq et al.* [1991].
[i] *Le* [1986].
[j] *Woodroof et al.* [1995].
[k] *Mai* [1995].

nier et al., 1986; *Peltzer and Tapponnier*, 1988]. The fact that sedimentation continued at rapid rates well after cessation of left-lateral movements along the WCTP faults may be related to thermal subsidence after the rifting phase. However, opening of several smaller basins, apparently related to E–W extension, is kinematically incompatible with left-lateral motion on the WCTP fault zones. This is the case of most of the N–S basins of central and northern Thailand (Figures 1b and 13a). In these basins, rifting, subsidence, and rapid sedimentation apparently started after cessation of sinistral movement on the faults: in the late Oligocene–early Miocene in most of the northern Gulf of Thailand and Chao Praya basins (Figure 13a and Table 4) and in the Miocene in the intramontane basins of northern Thailand (Figure 1b and Table 4). After localized rifting, regional subsidence also affected parts of these regions. Such subsidence was greater in the Gulf of Thailand, presently under sea level, than farther north. Together with northward younging of rifting, such northward decrease in the amount of subsidence implies diachronism in the onset of E–W extension, from the upper Oligocene to the south to early–middle Miocene in the north. It is possible that this diachronism was driven by reactivation in the opposite sense (right-lateral on NW–SE faults, left-lateral on NE–SW faults) of the Eocene–Oligocene strike–slip faults [e.g., *Le Dain et al.*, 1984; *Polachan et al.*, 1991]. Branching on these faults is clear for the normal fault–bounded Miocene to recent, intramontane basins (Figure 1b) and may account for the existence of the deep Phitsanulok basin (south of Sukhothai, Figures 1b and 13a), which appears to shortcut the wedge formed by the conjugate Wang Chao and Dien Bien Phu fault zones [*Polachan et al.*, 1991].

Diachronism of Strike–Slip Movement and Deformation Along the East Side of India

From ≈40 to ≈30 Ma the southern part of Indochina (or Sundaland) has been pushed towards the SE along the Wang Chao and Three Pagodas faults (Figures 13b and 13c). Rifting and extension in pull–apart and mismatch basins at the southeastern end of these strike–slip faults (Thai, Malay, and Mekong basins are T, Ma, and Me on Figure 13) have been in large part coeval with motion on them [*Tapponnier et al.*, 1986; *Peltzer and Tapponnier*, 1988]. Coevally, toward the north, shortening and thrusting with south–vergence seem to have occurred in the Eocene (≈36 Ma), whether in northern Tibet or in northern Indochina (Figure 13b) [*Lacassin et al.*, 1996]. N–S folding in the Simao basin and in northern Thailand and related conjugate striking faulting (Figure 1b) may have absorbed shortening on the west side of Indochina during extrusion (Figure 13c). The location of regions affected by shortening at that time is reminiscent of that of regions now undergoing shortening north and east of Tibet. N–S and E–W shortening, respectively, indeed characterize the contemporaneous tectonics of the Qilian Shan, at the north edge of the Tibet [*Tapponnier et al.*, 1990b; *Meyer*, 1991], and of the Lungmen Shan, along the western edge of South China. Early shortening and extrusion of the southernmost slice of Indochina apparently stopped somewhat after 30 Ma.

At the Oligo–Miocene boundary, as rapid left–lateral shear was occurring along the Ailao Shan–Red River shear zone [*Tapponnier et al.*, 1990a; *Schärer et al.*, 1990, 1994; *Leloup et al.*, 1995] concurrently with the opening of the South China Sea [*Briais et al.*, 1993] (Figure 13b), E–W extension, possibly linked with right–lateral reactivation of the WCTP faults, began to affect the southwestern part of Indochina (Figure 13d). At this time, southern Indochina was already located SE of the northeastern corner of the Indian indenter. The maximum horizontal stress due to the Indian push might thus have veered to nearly N–S in this region, allowing for E–W extension [*Tapponnier and Molnar*, 1976; *Tapponnier et al.*, 1982; *Le Dain et al.*, 1984; *Tapponnier et al.*, 1986; *Peltzer and Tapponnier*, 1988; *Huchon et al.*, 1994]. The uplift and cooling of the N–S metamorphic belt, that we document around 23 Ma (Figure 12), may have been related to such E–W extension and to normal faulting along the Sam Ngao fault. Note, however, that E–W shortening and N–S folding between 29 and 24 Ma may have caused some of the uplift of this belt [*Ahrendt et al.*, 1993].

Whatever the case, it seems clear that, as the Indian indenter kept penetrating into Asia (Figures 13b and 13d), Indochina suffered several radically different deformation phases in a rapidly changing kinematic framework [*Le Dain et al.*, 1984; *Tapponnier et al.*, 1986; *Leloup et al.*, 1995]. At the scale of the whole collision zone, India successively pushed toward the east several continent–size blocks along sinistral faults located farther and farther northward [*Tapponnier et al.*, 1982, 1986; *Peltzer and Tapponnier*, 1988]. The locus of major sinistral movement, as well as of the areas affected by shortening or extension, kept jumping toward the north (Figure 13). Our work on the faults of western Thailand supports the inference of northward diachronism in the onset and cessation of strike-slip movements on the east side of the collision zone (Table 5). Left–lateral motion occurred from at least 36 to 33 Ma, and 33 to 30 Ma along the Three Pagodas and Wang

Table 5. Summary of Avalaible Evidence on Duration of Strike-slip Motion E and SE of Tibet, and Fault Geometry with Respect to Indian Indenter

Fault Zone	Distance North of 5°N, km	Onset and End of sinistral motion, Ma	Distances at Onset and End of Sinistral Motion, km	Onset of Dextral Motion, Ma	Distance at Onset of Dextral Motion, km	Age Criteria
Three Pagodas fault	1700	≥36 to 33	≈ 1450 – 1050	≈ 23	≈ 400	radiometric dating
Wang Chao fault	1950	≥33 to 30	≈ 1450 – 1100	≈ 23	≈ 550	radiometric dating
Red River fault	2780	(35?) 26 to 17	≈ 2200 – 1200	≈ 5	≈ 500	radiometric dating
Xianshuihe fault	3170	≥15 to 0	≈ 1450 (onset)	future?		radiometric dating
Kunlun fault	3430	? to 0	?	future?		lacking
Haiyuan fault	3780	7 or 1.8 to 0	≈ 1560 (onset)	future?		morphological offsets

Distances are between India's NE corner and fault trace. See text and Figure 14 for discussion and references.

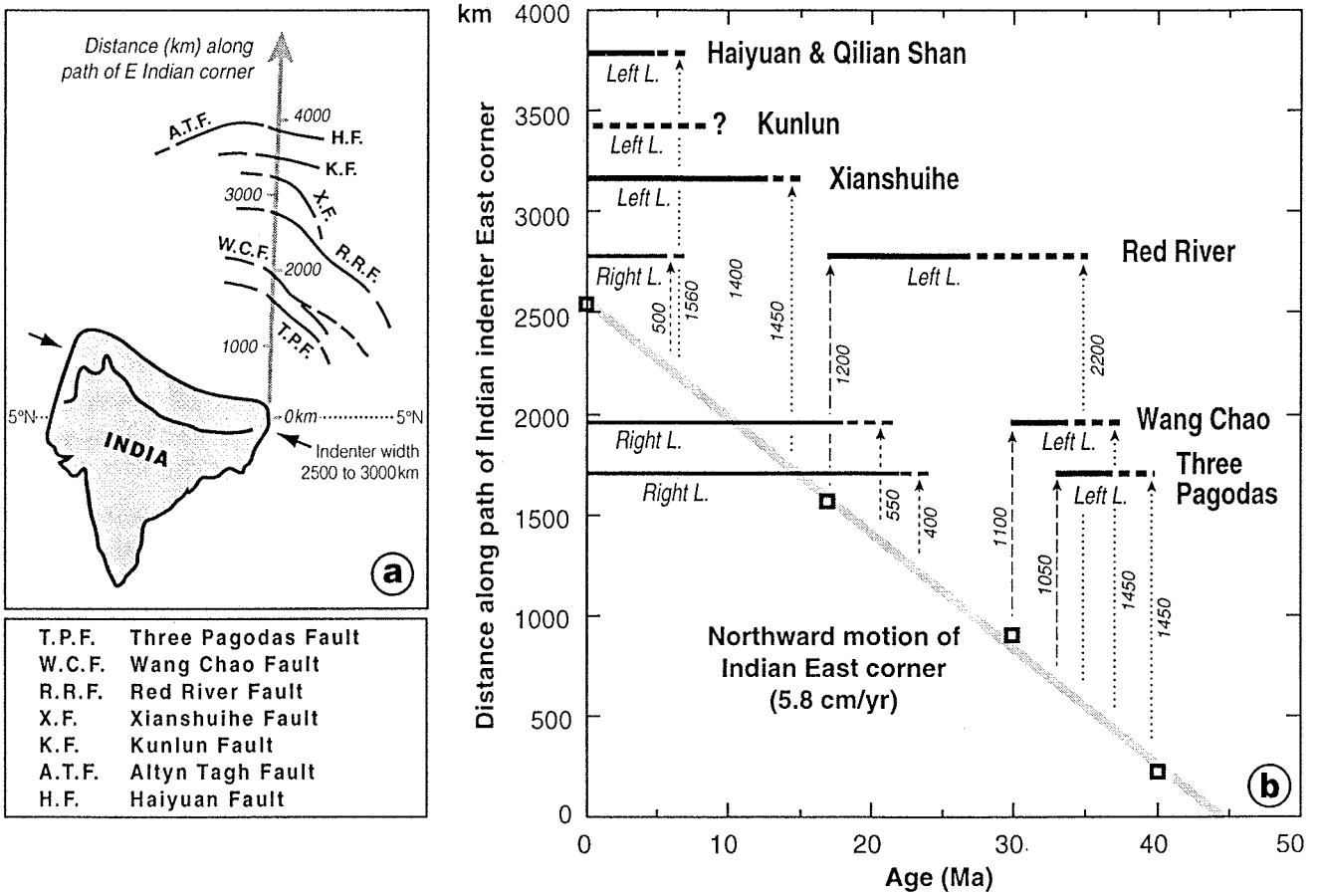

Figure 14. (a) Path of India within Asia (gray arrow). Present-day approximate distances between fault traces and eastern corner of Indian indenter at 5°N (44 Ma) are measured along that path (Table 5). Kinematic parameters for motion of India with respect to Asia as on Figure 13. (b) Location, in N–S geographical frame, of major strike–slip faults of eastern and southeastern Asia plotted as function of the ages of motion. Horizontal bars show periods of activity along each strike–slip fault (see discussion in text). Zero is taken at 5°N (position of NE Indian corner at about 44 Ma), and distances are measured along path of India (Figure 14a). Open squares and bold gray line (best fit line) show motion of India relative to Asia at 5.8 cm/yr. Arrowed lines show approximate distances between India and fault traces at times of probable onset of left–lateral motion (dotted), end of such motion (long dashes), and onset of right–lateral motion (short dashes).

Chao fault zones, respectively (Table 2 and Figure 13). Extrusion of Indochina occurred from at least 26 to 17 Ma (possibly as early as 35 Ma) along the Ailao Shan–Red River shear zone [*Schärer et al.*, 1990, 1994; *Leloup et al.*, 1995; *Harrison et al.*, 1996]. Farther north, left–lateral motion, still in progress, began at least 15 m.y. ago on the Xianshuihe fault [*Roger et al.*, 1995], and yet later along the Haiyuan fault, possibly as early as ≈7 m.y. ago [*Gaudemer et al.*, 1995] or as late as ≈1.8 Ma [*Burchfiel et al.*, 1991]. Accurate age constraints still lack for the Kunlun fault. The onset of E–W extension follows a comparable S–N diachronism. It occurred in the upper Oligocene in the Gulf of Thailand, in the Miocene in northern Thailand and probably in the Pliocene in Yunnan near the Red River fault [*Leloup et al.*, 1995].

Plotting such ages as a function of distance measured north of 5°N (Figure 14) shows that the approximate timing of left–lateral motion on the different faults lies roughly parallel to the path of the northeastern corner of the Indian indenter in a reference frame fixed to Eurasia. This gives quantitative support to diachronic activation, by the Indian indenter, of sinistral faults located farther and farther north. Apparently, left–lateral motion started on the Three Pagodas, Wang Chao, Xianshuihe, and Haiyuan faults, when the N–S distance between that corner and the traces of these faults became less than 1500–1600 km (Figure 14 and Table 5). If motion on the Red River started around 35 Ma [*Briais et al.*, 1993; *Schärer et al.*, 1994], the corresponding distance would have been greater (≈2200 km) (Figure 14 and Table 4). In addition, as distances between India's NE corner and the Three Pagodas, Wang Chao, and Red River faults fell below 1000–1200 km, the sinistral motion on them ceased (Figure 14 and Table 5). Finally, following a period of quiescence of about 10 m.y., the onset of right–lateral slip along these faults occurred when such distances became as small as 400–500 km (Figure 14 and Table 5).

The durations of motion along each of the left–lateral faults that bound the extruded continental blocks to the north and the timings of jumps from one fault system to the next one northward thus appears to be simply governed by the passage of the Indian indenter. Deformation apparently remained localized along each of these lithospheric faults during time spans of the order of 10 to 20 m.y. [*Leloup et al.*, 1995]. The time–space re-

lationships in Figure 14, suggest that fast slip on the sinistral faults initiates at distances between 1 and 1/2 the width of the indenter and stop when these distances become smaller than ≈1/3 this width. Such geometrical relationships are roughly in keeping with the results of plasticine indentation experiments [*Tapponnier et al.*, 1986; *Peltzer and Tapponnier*, 1988], even though shortening by crustal thickening of the western part of the extruded blocks ought to make such distances smaller in nature. The distance at which right-lateral faulting starts is comparable to the maximum distance between the Himalayan arc and its chord as might be expected if such faulting reflects decoupling between thickened crust along the north edge of India and blocks pushed eastward not far north of it [*Armijo et al.*, 1986, 1989]. Although the time-space diagram of Figure 14 is preliminary, the evidence at hand supports the idea that diachronism in the eastward extrusion of continent-size blocks was important throughout the India-Asia collision [*Tapponnier et al.*, 1982; *Armijo et al.*, 1989; *Leloup et al.*, 1995] but not domino or bookshelf models [e.g., *Cobbold and Davy*, 1988; *England and Molnar*, 1990] that require coeval block rotation.

Appendix: Description of Dated Samples and $^{40}Ar/^{39}Ar$ Results

Location of Dated Samples and Analytical Procedure

Samples were taken in the Lansang gneisses along the Tak–Mae Sot highway (TL3, TL7, TL8) and along Huai Lansang (TA34) (Figures 3 and 4). We sampled the Chiang Mai–Lincang belt along the Sam Ngao–Bhumibol dam section (TL13, TL14, TL16, Figure 2) and on the outcrop 10 km west of Ban Tak (TL17, Figure 2). One additional sample (TL19, Figures 1b and 2) of this belt has been collected south of the Lansang gneisses, about 40 km S of Tak (99°11'E–16°31'N). An orthogneiss sample has been taken at Khao Chon Kai (99°24'–14°08'N), NW of Kanchanaburi within the Three Pagodas fault zone (TL21, Figure 1b). Progressive step–heating on selected mineral size-fraction populations was applied to TL3, 8, 13, 14, 19, while heating with a continuous laser was applied to TL7, 16, 17, TL21, both at the University of Montpellier. The procedure used, such as correction parameters, is fully described by *Monié et al.* [1994] and *Maluski et al.* [1995b]. Progressive step–heating was applied to the TA34 biotite at T.M. Harrison's laboratory in UCLA. The K–feldspar from TA34 was measured at the University of Clermont Ferrand N. Arnaud's laboratory using the heating procedure that permits to retrieve and model its thermal history [*Harrison et al.*, 1991; *Lovera et al.*, 1991].

Description of Samples and Dating Results

Lansang gneisses (samples TL3, TL7, TL8, TA 34). TL7 (Figure 4) is a coarse-grained augen–gneiss, with quartz, feldspar, biotite, muscovite, few hornblende, epidote, and calcite. TL8 (Figure 4) is a fine–grained orthogneiss. In these samples, biotites crystallized during, or late in, the main episode of deformation and outline the foliation and the stretching lineation. Quartz is recrystallized and feldspar porphyroclasts (plagioclase) form augen and polycristalline aggregates with elongated tails. TL3 (equivalent to TA39, Figure 8c) is a fine–grained gneiss bearing quartz, feldspar, biotite and some muscovite, taken from the southwestern part of the Tak–Mae Sot road section (Figure 4). In this sample, biotite and muscovite occur as small grains outlining the lineation and deformed within left–lateral shear planes (Figure 8d). TA34, coming from Huai Lansang (Figures 3 and 6), is a C/S orthogneiss bearing feldspar, biotite and quartz.

For TL3 biotite the plateau age, calculated for 64% of ^{39}Ar released, is 33.1 ±0.4 Ma (Figure 9a). The inverse correlation plot yields the same age (33 ±0.3 Ma) with a $^{40}Ar/^{36}$ ratio of 280 ± 10 close to the atmospheric ratio (295.5). More scattered data are obtained for the last 35% of the ^{39}Ar release, with ages ranging from 30.8 to 33.7 Ma.

The age spectrum for TL7 (continuous laser dating on one single biotite grain) is characterized by excess argon during the first half of degassing, giving ages ranging from 75 to 33 Ma (Figure 9b). In the second part of the spectrum, until final melting of the sample, ages are scattered between 31.6 and 34.8 Ma. The age, calculated for the last 40% of argon release, is 33.0 ±0.2 Ma. Clustering of precluded the determination of any significant inverse correlation isochron.

For TL8 biotite, the first part of the spectrum (low temperature steps up to 800°C) is the most homogeneous (Figure 9c) and the age calculated for ≈50% of ^{39}Ar release is 31.3 ±0.7 Ma. Comparable values are obtained for the total integrated age (31.2 ±0.7 Ma, 100% of argon release) and from the inverse correlation diagram (31.4 ±0.3 Ma) with a $^{40}Ar/^{36}Ar$ ratio close to the atmospheric value.

The TA34 biotite gives a plateau age of 30.6 ±0.3 Ma calculated for 75% of Ar degassing (Figure 10a) similar to the total age (30.5 ±0.5 Ma) and to the inverse isochron age on all steps (31.4 ±1.8 Ma, initial ratio close to the atmospheric value, Table 1). The age spectrum of TA34 K–feldspar shows an initial rise in the first 10% of Ar release and a first plateau between 23 and 24 Ma (Figure 10a). Then the ages increase progressively and culminate in a bump at 33 Ma (80% of Ar release), suggestive of excess argon trapped in some of the most retentive domains of the sample [*Foster et al.*, 1990]. The remaining steps (last 16% of degassing) correspond to younger ages defining two very rough plateau at 30.5 and 31.5 Ma.

Three Pagodas fault zone (sample TL21). TL21 is an orthogneiss bearing recrystallized quartz, K–feldspar, and plagioclase. Staurolite occurs as undeformed crystals. Biotite and muscovite lie in the foliation. Biotite, analyzed with continuous laser heating, yields a composite age spectrum (Figure 9d). Low to intermediate temperature increments correspond to scattered ages starting at 10 Ma and increasing up to 36.8 Ma. Then the ages decrease slightly and define a plateau at 33.4 ±0.3 Ma for the last 50% of argon release (900°C to melting). The inverse correlation plot confirms this age (32.6 ±0.5), with a $^{40}Ar/^{36}Ar$ ratio of 320 ± 10 reflecting a slight excess argon component (Table 1).

Metamorphic rocks SSE of the Lansang gneisses (sample TL19). TL19 (Figure 2) is a biotite–amphibole bearing gneiss. The amphibole shows a well-defined plateau at 446 ± 5 Ma (Figure 11a). The dated biotite is a mix of chlorite with less weathered Biotite. Its age spectrum does not allow significant age calculation (total age is ≈359 ± 6 Ma) but suggests an old Paleozoic age in the same range as the amphibole (Figure 11b).

Metamorphic rocks between Lansang gneisses and Bhumibol dam (TL 13, TL14, TL16, TL17). TL13 and TL14 (Figure 2) are marbles with thin layers of quartz and scattered biotite and muscovite. Both samples yield age spectrum with a release of excess argon during low temperature steps (Figures 11c and 11d). The ages, calculated for interme-

diate–to high–temperature steps, are 29.0 ±1 Ma and 27.9 ±3 Ma for TL13 and TL14, respectively (Figures 11c and 11d), Inverse correlation diagrams give slightly younger ages of 27.3 ±0.6 Ma and 26 ±0.5 Ma for TL13 and TL14, respectively, with $^{40}Ar / ^{36}Ar$ ratios close to the atmospheric value (Table 1).

TL16 (Figure 2) is a biotite, muscovite bearing augengneiss and TL17 (Figure 2) a migmatitic gneiss. Continuous laser heating on single biotite grains give very comparable age spectra (Figures 11e and 11f) with, as for TL13 and TL14, excess Ar at low–temperature steps and then a well–defined plateau. The plateau age of TL16 is 23.2 ±0.1 Ma (Figure 11e), with a similar value (23 ±0.6 Ma) from the inverse correlation (Table 1). The age of TL17 (last 50% of argon release) is 25.4 ±0.8 Ma (Figure 11f) while the inverse isochron age is 27.2 ±6 Ma, with a $^{40}Ar / ^{36}Ar$ ratio of 226 (Table 1).

Acknowledgments. Field work was carried out with the logistic support of the Thailand Department of Mineral Resources (DMR). We thank S. Bunopas and the director of the DMR for providing this support. T. M. Harrison and N. Arnaud are gratefully acknowledged for their help in dating some samples of the Lansang gneisses and for discussing the results and improving the interpretations presented in this paper. We thank J. P. Burg for a constructive review. We also benefited from discussions with A. Briais, J. Besse, and J. R. Kienast. We finally acknowledge financial support by programs Mecalith and Tectoscope of the Institut National des Sciences de l'Univers (INSU) and by URA 1093 and 5563 of the Centre National de la Recherche Scientifique (CNRS). This is IPGP contribution 1462. Complementary data (photographs, analytical results) may be found on IPGP web site (http://www.igpp.jussieu.fr/depts/tecto.html).

References

Ahrendt, H., C. Chonglakmani, B. T. Hansen, and D. Helmcke, Geochronological cross section through northern Thailand, *J. SE Asia Earth Sci.*, *8*, 207-217, 1993.

Allen, C. R., A. R. Gillespie, Y. Han, K. E. Sieh, B. Zhang, and C. Zhu, Red River and associated faults, Yunnan province, China: Quaternary geology, slip rates, and seismic hazard, *Geol. Soc. Am. Bull.*, *95*, 686-700, 1984.

Armijo, R., P. Tapponnier, J. L. Mercier, and H. Tonglin, Quaternary extension in southern Tibet: Field observations and tectonic implications, *J. Geophys. Res.*, *91*, 13,803-13,872, 1986.

Armijo, R., P. Tapponnier, and H. Tonglin, Late Cenozoic right–lateral strike–slip faulting in southern Tibet, *J. Geophys. Res.*, *94*, 2787-2838, 1989.

ASEAN Council on Petroleum, Tertiary sedimentary basins of the Gulf of Thailand and South China Sea: Stratigraphy, structure and hydrocarbon occurrences, report, Jakarta, 1981.

Barr, S. M., and A. S. Mac Donald, Nan river suture zone, northern Thailand, *Geology*, *15*, 907-910, 1987.

Baum, F., E. Von Brau, L. Hahn, A. Hess, K. E. Koch, G. Kruse, H. Quarch, and M. Siebenhüner, On the geology of northern Thailand, *Beih. Geol. Jahrb.*, *102*, 23 pp., 1970.

Beckinsale, R. D., S. Suensilpong, S. Nakapadungrat, and J. N. Walsh, Geochronology and geochemistry of granite magmatism in Thailand in relation to a plate tectonic model, *J. Geol. Soc. London.*, *136*, 529-540, 1979.

Berthé, D., P. Choukroune, and P. Jegouzo, Orthogneiss, mylonite and non-coaxial deformation of granites: The example of the South Armorican shear zone, *J. Struct. Geol.*, *1*, 31-42, 1979a.

Berthé, D., P. Choukroune, and D. Gapais, Orientations préférentielles du quartz et orthogneissification progressive en régime cisaillant: L'exemple du cisaillement sud-armoricain, *Bull. Minéral.*, *102*, 265-272, 1979b.

Besse, J., and V. Courtillot, Paleogeographic maps of the continents bordering the Indian Ocean since the early Jurassic, *J. Geophys. Res.*, *93*, 11791-11808, 1988.

Braun, E. V., C. Besang, W. Eberle, W. Harre, H. Kreuzer, H. Lenz, P. Muller, and I. Wendt, Radiometric age determinations of granites in northern Thailand, *Geol. Jahrb.*, *B21*, 171-204, 1976.

Braun, E. V., L. Hahn, and H. D. Maronde, Geological map of Thailand, scale 1:250,000, sheet Amphoe Li 6, Fed. Inst. for Geosci. and Nat. Ressour., Hannover, 1981.

Briais, A., P. Patriat, and P. Tapponnier, Updated interpretation of magnetic anomalies and seafloor spreading stages in the South China Sea, implications for the Tertiary tectonics of SE Asia, *J Geophys. Res.*, *98*, 6299-6328, 1993.

Brunel, M., Quartz fabrics in shear-zone mylonite: Evidence for a major imprint due to late strain increments, *Tectonophysics*, *64*, T33-T44, 1980.

Bunopas, S., Geological map of Thailand, scale 1:250,000, sheet Phitsanulok NE 47-15, Geol. Surv. Div., Dep. of Miner. Resour., Bangkok, 1974.

Bunopas, S., Geological map of Thailand, scale 1:250,000, sheet Suphan Buri ND 47-7, Geol. Surv. Div., Dep. of Miner. Resour., Bangkok, 1976.

Bunopas, S., Paleogeographic history of western Thailand and adjacent parts of Southeast Asia: A plate tectonics interpretation, Ph.D thesis, 810 pp., Victoria Univ. of Wellington, Wellington, New Zealand, 1981.

Bunopas, S., and P. Vella, Opening of the Gulf of Thailand: Rifting of continental Southeast Asia, and late Cenozoic tectonics, *J. Geol. Soc. Thailand*, *6*, 1-12, 1983.

Burchfiel, B. C., P. Zhang, Y. Wang, W. Zhang, D. Jiao, F. Song, Q. Deng, P. Molnar, and L. H. Royden, Geology of the Haiyuan fault zone, Ningxia–Hui autonomous region, China, and its relation to the evolution of the northeastern margin of the Tibetan Plateau, *Tectonics*, *10*, 1091-1110, 1991.

Campbell, K. V., Structural setting and metamorphic grade of the Lansang gneiss, *Geol. Soc. Thailand Newsl.*, *6*, 32-45, 1973.

Campbell, K. V., Metamorphic and deformational events recorded in the Lansang gneiss, report, Chiang Mai Univ., Chiang Mai, 1976.

Cobbing, E. J., P. E. Pitfield, D. P. F. Darbyshire, and D. I. J. Mallick, *The Granites of the South-East Asian Tin Belt, Overseas Memoir of the British Geological Survey*, vol. 10, 369 pp., Her Majesty's Stn Off., Norfolk, England, 1992.

Cobbold, P., and P. Davy, Indentation tectonics in nature and experiment, 2, Central Asia, *Bull. Inst. Univ. Uppsala*, *14*, 143-162, 1988.

Cobbold, P., and H. Quinquis, Development of sheath folds in shear regime, *J. Struct. Geol.*, *2*, 119-126, 1980.

Department of Mineral Resources, Geological Map of Thailand, scale 1:1,000,000, R. Thai Surv. Dep., Bangkok, 1982.

Ducrocq, S., Etude Biochronologique des bassins continentaux Tertiaires du Sud-Est Asiatique: Contribution des mammifères, doctorat thesis, 242 pp., Univ. of Montpellier, Montpellier, France, November 1992.

Ducrocq, S., E. Buffetaut, H. Buffetaut-Tong, Y. Chaimanee, J. J. Jaeger, and V. Suteethorn, Age and correlations of the Neogene continental basins from Thailand, paper presented at 7th Regional Conference on Geology, Miner. and Energy Resour. of SE Asia (GEOSEA VII), Bangkok, Nov., 5-8, 1991.

Dunning, G. R., A. S. Macdonald, and S. M. Barr, Zircon and monazite U-Pb dating of the Doi Inthanon core complex, northern Thailand: Implications for extension within the Indosinian orogen, *Tectonophysics*, *251*, 197-213, 1995.

Earth Sciences Research Division, Geological map of the Socialist Republic of the Union of Burma, scale 1:1,000,000, Rangoon, 1977.

England, P., and P. Molnar, Right-lateral shear and rotation as the explanation for strike-slip faulting in eastern Tibet, *Nature*, *344*, 140-142, 1990.

Foster, D. A., T. M. Harrison, P. Copeland, and M. T. Heitzler, Effects of excess argon within large diffusion domains on K-feldspar age spectra, *Geochim. Cosmochim. Acta*, *54*, 1699-1708, 1990.

Gaudemer, Y., and P. Tapponnier, Ductile and brittle deformations in the northern Snake Range, Nevada, *J. Struct. Geol.*, *9*, 159-180, 1987.

Gaudemer, Y., P. Tapponnier, B. Meyer, G. Peltzer, S. Guo, Z. Chen, H. Dai, and I. Cifuentes, Partitioning of crustal slip between linked, active faults in the eastern Qilian Shan, and evidence for a major seismic gap, the "Tianzhu gap," on the western Haiyuan Fault, Gansu (China), *Geophys. J. Int.*, *120*, 599-645, 1995.

Hahn, L., K. E. Koch, H. Wittekindt, W. Adelhardt, and A. Hess, Outline of the geology and the mineral potential of Thailand, *Geol. Jahrb.*, *B59*, 3-59, 1986.

Hamilton, W., Tectonics of the Indonesian region, *U.S. Geol. Surv. Prof. Pap.*, *1078*, 345 pp., 1979.

Hanmer, S., and C. Passchier, Shear-sense indicators: A review, *Pap. Geol. Surv. Can. 90-17*, 72 pp., 1991.

Harrison, T. M., M. T. Heizler, and O. M. Lovera, $^{40}Ar/^{39}Ar$ results for alkali feldspar containing diffusion domains with differing activation energy, *Geochim. Cosmochim. Acta*, *55*, 1435-1448, 1991.

Harrison, T. M., Chen W., P. H. Leloup, F. J. Ryerson, and P. Tapponnier, An early Miocene transition in deformation regime within the Red River fault zone, Yunnan, and its significance for Indo-Asian tectonics, *J. Geophys. Res.*, *97*, 7159-7182, 1992.

Harrison, T. M., P. H. Leloup, F. J. Ryerson, P. Tapponnier, R. Lacassin, and Chen W., Diachronous initiation of transtension along the Ailao Shan–Red River shear zone, Yunnan and Vietnam, in *The Tectonics of Asia*, edited by Harrison, T. M., and A. Yin, pp. 208-226, Cambridge Univ. Press, New York, 1996.

Huchon, P., X. Le Pichon, and C. Rangin, Indochina peninsula and the collision of India and Eurasia, *Geology*, *22*, 27-30, 1994.

Hutchinson, C. S., *Geological Evolution of SE Asia*, Oxford Monographs on Geology and Geophysics, vol. 13, 368 pp., Clarendon, Oxford, England, 1989.

Lacassin, R., and M. Mattauer, Kilometre-scale sheath fold at Mattmark and implications for transport direction in the Alps, *Nature*, *316*, 739-742, 1985.

Lacassin, R., P. H. Leloup, and P. Tapponnier, Bounds on strain in large Tertiary shear zones of SE Asia from boudinage restoration, *J Struct. Geol.*, *15*, 677-692, 1993.

Lacassin, R., U. Schärer, P. H. Leloup, N. Arnaud, P. Tapponnier, X. Liu, and L. Zhang, Tertiary deformation and metamorphism SE of Tibet: The folded Tiger-leap décollement of NW Yunnan, China, *Tectonics*, *15*, 605-622, 1996.

Le Dain, A. Y., P. Tapponnier, and P. Molnar, Active faults and tectonics of Burma and surrounding regions, *J. Geophys. Res.*, *89*, 453-472, 1984.

Leloup, P. H., and J. R. Kienast, High temperature deformation in a major Tertiary ductile continental strike-slip fault: Evidence of shear heating at lithospheric scale?, *Earth Planet. Sci. Lett.*, *118*, 213-234, 1993.

Leloup, P. H., T. M. Harrison, F. J. Ryerson, W. Chen, L. Qi, P. Tapponnier, and R. Lacassin, Structural, petrological and thermal evolution of a Tertiary ductile strike-slip shear zone, Diancang Shan, Yunnan, *J. Geophys. Res.*, *98*, 6715-6743, 1993.

Leloup, P. H., R. Lacassin, P. Tapponnier, D. Zhong, X. Liu, L. Zhang, S. Ji, and P. T. Trinh, The Ailao Shan-Red River shear zone (Yunnan, China), Tertiary transform boundary of Indochina, *Tectonophysics*, 251, 3-84, 1995.

Le, V. K., The structure of the Mekong trough, *Int. Geol. Rev.*, *28*, 87-95, 1986.

Liew, T. C., and R. W. Page, U-Pb zircon dating of granitoid plutons from the west coast province of Peninsular Malaysia, *J. Geol. Soc. London*, *142*, 515-526, 1985.

Liu, C., J. Zhu, X. Xu, X. Chu, D. Cai, and Y. Pin, Study on the characteristics of Linchang composite granite batholith in west Yunnan, *Geol. of Yunnan*, *8*, 189-204, 1989.

Lovera, O. M., F. M. Richter, and T. M. Harrison, Diffusion domains determined by ^{39}Ar released during step heating, *J. Geophys. Res.*, *96*, 2057-2069, 1991.

Mac Donald, A. S., S. M. Barr, G. R. Dunning, and W. Yaowanoiyothin, The Doi Inthanon metamorphic core complex in NW Thailand: Age and tectonic significance, *J. SE Asia Earth Sci.*, *8*, 117-125, 1993.

Mahawat, C., M. P. Atherton, and M. S. Brotherton, The Tak batholith, Thailand: The evolution of contrasting granite types and implications for tectonic setting, *J. SE Asia Earth Sci.*, *4*, 11-27, 1990.

Mai, T. T., Seismic-stratigraphic studies of the continental shelf of southern Vietnam, *J. Petrol. Geol.*, *18*, 345-354, 1995.

Malavieille, J., Extensional shearing deformation and kilometer-scale "a"-type folds in a cordilleran metamorphic core complex (Raft River mountains, northwestern Utah), *Tectonics*, *6*, 423-448, 1987.

Maluski, H., C. Lepvrier, D. Roques, N. V. Vuong, P. V. Quynh, and C. Rangin, $^{40}Ar/^{39}Ar$ ages in the Danang–Dailoc plutono-metamorphic complex (Central Vietnam): Overprinting process of Cenozoic over Indosinian thermotectonic episodes, paper presented at the Cenozoic evolution of the Indochina peninsula conference, Hanoi–Do Son, Vietnam, 1995a.

Maluski, H., C. Coulon, M. Popoff, and P. Baudin, $^{40}Ar/^{39}Ar$ chronology, petrology and geodynamic setting of Mesozoic to early Cenozoic magmatism from the Benue Trough, Nigeria, *J. Geol. Soc. London*, *152*, 311-326, 1995b.

Martelet, G., Estimation d'un minimum de déplacement ductile sur la faille de Wang Chao (Thailande) au Tertiaire. Conditions P-T du métamorphisme engendré, report, Univ. de Paris 7, 1994.

Meyer, B., Mécanismes des grands tremblements de terre et du raccourcissement crustal oblique au bord Nord-Est du Tibet, Doctorat thesis, 129 pp., Univ. de Paris 6, 1991.

Monié, P., J. Soliva, M. Brunel, and H. Maluski, Les cisaillements mylonitiques du granite de Millas (Pyrénées, France): Age Crétacé $^{40}Ar/^{39}Ar$ et interprétation tectonique, *J. Geol. Soc. London*, *165*, 559-571, 1994.

Mouret, C., Geological history of northeastern Thailand since the Carboniferous. Relations with Indochina and Carboniferous to early Cenozoic evolution model, in *Proceedings of the International Symposium on Stratigraphic Correlation of Southeast Asia*, edited by P. Angsuwathana et al., pp. 132-158, Dep. of Miner. Resour., Bangkok, 1994.

Patriat, P., and J. Achache, India-Eurasia collision chronology has implications for crustal shortening and driving mechanism of plates, *Nature*, *311*, 615-621, 1984.

Peltzer, G., and P. Tapponnier, Formation and evolution of strike–slip faults, rifts, and basins during India–Asia collision: An experimental approach, *J. Geophys. Res.*, *93*, 15,085-15,117, 1988.

Pigott, J. D., and N. Sattayarak, Aspects of sedimentary basin evolution assessed through tectonic subsidence analysis. Example: northern Gulf of Thailand, *J. SE Asia Earth Sci.*, *8*, 407-420, 1993.

Piyasin, S., Geological map of Thailand, scale 1:250,000, sheet Uttaradit NE 47-11, Geol. Surv. Div., Dep. of Miner. Resour., Bangkok, 1974.

Platt, J. P., and R. L. M. Vissers, Extensional structures in anisotropic rocks, *J. Struct. Geol.*, *2*, 397-410, 1980.

Polachan, S., S. Pradidtan, C. Tongtaow, S. Janmaha, K. Intarawijitr, and C. Sangsuwan, Development of Cenozoic basins in Thailand, *Mar. Pet. Geol.*, *8*, 84-97, 1991.

Remus, D., M. Webster, and K. Keawkan, Rift architecture and sedimentology of the Petchabun intermontane basin, central Thailand, *J. SE Asia Earth Sci.*, *8*, 421-432, 1993.

Roger, F., S. Calassou, J. Lancelot, J. Malavieille, M. Mattauer, Z. Xu, Z. Hao, and L. Hou, Miocene emplacement and deformation of the Konga Shan granite (Xianshui He Fault zone, west Sichuan, China): Geodynamical implications, *Earth Planet. Sci. Lett.*, 130, 201-216, 1995.

Schärer, U., P. Tapponnier, R. Lacassin, P. H. Leloup, D. Zhong, and S. Ji, Intraplate tectonics in Asia: A precise age for large-scale Miocene movement along the Ailao Shan-Red River shear zone, China, *Earth Planet. Sci. Lett.*, *97*, 65-77, 1990.

Schärer, U., L. Zhang, and P. Tapponnier, Duration of strike-slip movements in large shear zones: The Red River belt, China, *Earth Planet. Sci. Lett.*, *126*, 379-397, 1994.

Sengör, A. M. C., and K. J. Hsü, The cimmerides of eastern Asia: History of the eastern end of Palaeo-Tethys, *Mém. Soc. Géol. Fr.*, *147*, 139-167, 1984.

Siribhakdi, K., S. Salyapongse, and V. Suteetorn, Geological map of Thailand, scale 1:250,000, sheet Tavoy ND 47-6, Geol. Surv. Div., Dep. of Miner. Resour., Bangkok, 1985.

Sukto, P., V. Suteethorn, S. Boripatgosol, A. Meesok, and S. Sareerat, Geological map of Thailand 1:250 000, Sheet Moulmein NE 47-14, Geological Survey Division, Department of Mineral Resources, Bangkok, Thailand, 1984.

Tapponnier, P., and P. Molnar, Slip-line field theory and large-scale continental tectonics, *Nature*, *264*, 319-324, 1976.

Tapponnier, P., and P. Molnar, Active faulting and tectonics in China, *J. Geophys. Res.*, *82*, 2905-2930, 1977.

Tapponnier, P., G. Peltzer, R. Armijo, A.-Y. Le Dain, and P. Cobbold, Propagating extrusion tectonics in Asia: New insights from simple experiments with plasticine, *Geology*, *10*, 611-616, 1982.

Tapponnier, P., G. Peltzer, and R. Armijo, On the mechanics of the collision between India and Asia, in *Collision Tectonics*, edited by M. P. Coward, and A. C. Ries, *Geol. Soc. Spec. Publ.*, 19, 115-157, 1986.

Tapponnier, P., R. Lacassin, P. H. Leloup, U. Schärer, D. Zhong, X. Liu, S. Ji, L. Zhang, and J. Zhong, The Ailao Shan–Red River metamorphic belt: Tertiary left-lateral shear between Indochina and South China, *Nature*, *343*, 431-437, 1990a.

Tapponnier, P., et al., Active thrusting and folding in the Qi Lian

Shan, and decoupling between the upper crust and mantle in northeastern Tibet, *Earth Planet. Sci. Lett.*, *97*, 382-403, 1990b.

Van Den Driessche, J., and J. P. Brun, Rolling structure at large strain, *J. Struct. Geol.*, *9*, 691-704, 1987.

Woodroof, P. B., T. L. Nguyen, and S. C. Bergman, Structure and stratigraphy in the northern Nam Con Son basin, Vietnam, paper presented at the Cenozoic evolution of the Indochina peninsula conference, Hanoi–Do Son, Vietnam, 1995.

A. Charoenravat, S. Chuaviroj, C. Hinthong, and K. Siribhakdi, Geological Survey Division, Department of Mineral Resources, Bangkok, Thailand.

R. Lacassin, P. H. Leloup, and P. Tapponnier, Laboratoire de Tectonique, Mécanique de la Lithosphère; Institut de Physique du Globe de Paris, 4 Place Jussieu, 75252 Paris CX05, France. (e-mail: lacassin@ipgp.jussieu.fr)

H. Maluski, Laboratoire de Géochronologie Géochimie et Pétrologie, URA 5563 CNRS Université Montpellier 2, 34095 Montpellier, France. (e-mail: maluski@dstu.univ-montp2.fr)

(Received July 1, 1996; revised December 2, 1996;
accepted December 9, 1996.)

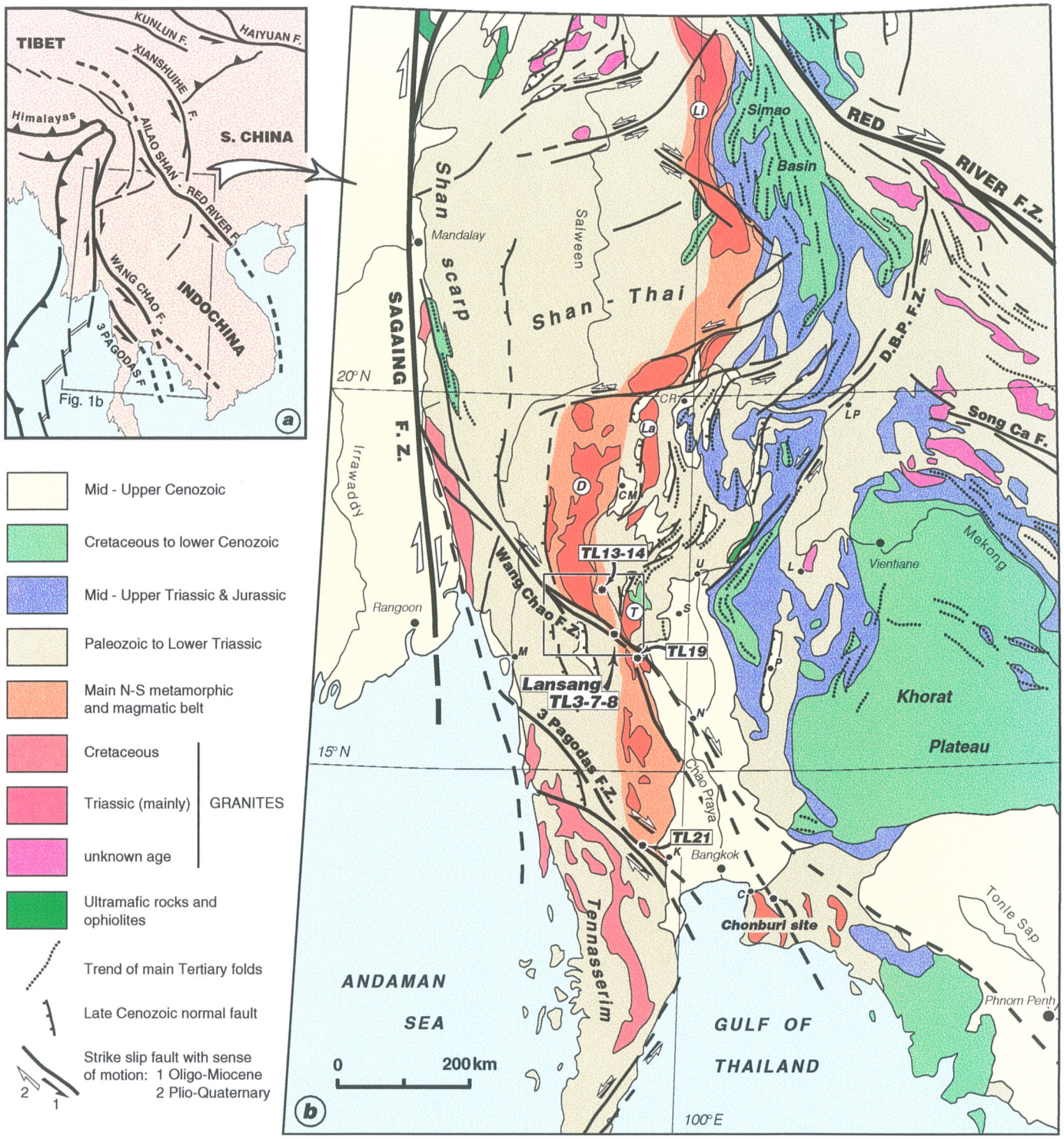

Figure 1. Structural and geological sketches of SE Asia showing location of studied areas in northwestern Thailand. (a) Map of major Cenozoic faults of mainland SE Asia and eastern Tibet [after Leloup et al., 1995]. Arrows show senses of finite motion on strike–slip faults. Boxed area refers to Figure 1b. (b) Structural sketch map drawn from 1:5,000,000 scale geological map of Asia [*Department of Mineral Resources, 1982*] , Landsat and Spot satellite images, ONC (Operational Navigation Chart) and TPC (Tactical Pilot Chart) topographic maps. Geological offsets (solid arrows) are inferred to have occurred coevally with Tertiary extrusion of Indochina [*Tapponnier et al., 1986, 1990a; Leloup et al., 1995*] . Present–day senses of motion (open arrows), deduced from morphological offsets and seismicity, are opposite to finite geological offsets [*Le Dain et al., 1984*] . Trends of main Tertiary folds (dotted lines) are deduced from geological maps and satellite imagery. TL3-7-8, TL13-14, TL19, and TL21 refer to samples dated using $^{40}Ar/^{39}Ar$ ttechnique (see also Figure 2). DBPFZ is Dien Bien Phu fault zone; Li, La, D, and T, Lincang, Lampang, Doi Inthanon, and Tak metamorphic or magmatic massifs; U, Uttaradit; CM, Chiang Mai; CR, Chiang Rai; S, Sukhothai; N, Nakhon Sawan; K, Kanchanaburi; C, Chonburi; L, Loei; P, Petchabun; M, Moulmein; LP, Luang Prabang. Boxed area refers to Figure 2.